THE $O^{16}(p,\gamma)F^{17}$ REACTION

by

LYLE PURMAL ROBERTSON

A THESIS SUBMITTED IN PARTIAL FULFILMENT OF

THE REQUIREMENTS FOR THE DEGREE OF

MASTER OF ARTS

in the Department

of

PHYSICS

We accept this thesis as conforming to the
standard required from candidates for the
degree of

MASTER OF ARTS

Members of the department of Physics

THE UNIVERSITY OF BRITISH COLUMBIA

November, 1957

ABSTRACT

The differential cross section for direct radiative capture of protons by O^{16} has been measured using ice targets of known thickness and 800 kev. protons. The differential cross section for the gamma ray transition to the first excited state in F^{17} was found to be $(10.4 \pm 1.3) \times 10^{-32}$ cm^2. per steradian at $90°$ to the incident proton beam direction. At the same energy, the ratio of the differential cross section at $90°$ for transitions to the ground state to that for transitions to the first excited state in F^{17} was found to be 0.14 ± 0.03.

The energy of the first excited state in F^{17} was determined by measuring the energy of the gamma ray from this level to the ground state. This method is difficult because of the presence of positron annihilation radiation of the same energy, within experimental errors, from the decay of F^{17}. The first excited state energy was also measured by noting the difference between the capture gamma rays to this state and to the ground state. The energy of this level was found to be 0.50 ± 0.01 Mev. in agreement with the results of Marion and Bonner (55) and with earlier results obtained in this laboratory (Warren et. al., (54).

An attempt to confirm that the source of the 873 kev. radiation from proton bombardment of natural oxide targets above 1.8 Mev. bombarding energy was the $O^{17}(p, p', \gamma)O^{17}$ reaction, was made using separated O^{16} and O^{17} targets. The results were inconclusive due to the small percentage of oxygen that stuck to the targets and to the presence of several contaminants.

ACKNOWLEDGEMENTS

TABLE OF CONTENTS

LIST OF ILLUSTRATIONS

CHAPTER I

INTRODUCTION

Shell model predictions indicate that the F^{17} nucleus can be considered as a single proton moving in the potential of the doubly closed shell O^{16} core. This system is therefore a simple one to consider theoretically and should lend itself to a quantitative test of shell model predictions. Comparison with its mirror nucleus O^{17} should indicate a one to one correspondence between level energies (corrected for coulomb and neutron-proton mass difference effects) and spin and parity values.

The shell model predicts that the ground state of both O^{17} and F^{17} should be a $D5/2^+$ level consisting of the odd nucleon with its spin aligned parallel to the orbital angular momentum. Experimental results are consistent with $D_{5/2}^+$ for both ground states. The O^{17} ground state spin has been measured directly by Alder and Yu (51) and the assumption that the F^{17} ground state spin is 5/2 is consistent with the allowed β^+ transition to O^{17} and with O^{16} (d,n) stripping data (Ajzenburg, 51). The first excited state of the mass 17 system appears not to be the $D_{3/2}$ member of the ground state doublet but to be an $S_{1/2}^+$ level of the odd nucleon. This is consistent with present shell model predictions. The experimental evidence comes from stripping angular distributions of $O^{16}(d,p)O^{17}$ (Burrows et al, 50) and $O^{16}(d,n)F^{17}$ (Ajzenburg, 51). Additional evidence for O^{17} spins

is available from angular correlation between protons and γ-rays from the first excited state (Thirion, 53) and from internal conversion measurements on the same γ-rays which indicate an E-2 transition (Thomas and Lauritsen, 52).

This consistency between the shell model predictions and experimental evidence for level parameters of ground state and the first excited state of F^{17} suggests that a calculation for the $O^{16}(p,\gamma)F^{17}$ reaction parameters assuming this simple configuration for F^{17}, should give reasonable results. Theoretical calculations for the cross section and angular distribution of this reaction are being made by a California Institute of Technology group (private communication from N. Tanner). A direct radiative capture process is being assumed, consistent with the results of Warren et al (54) that the γ-radiation from $O^{16}(p,\gamma)$ was non-resonant in the region E_p 0.9 to 2.1 Mev. Since a detailed comparison between the theoretical calculations and accurate experimental results should provide a sensitive check on the assumed models it was felt that more accurate data on the cross section and angular distribution of the gamma radiation would be of value at this time.

The $O^{16}(p,\gamma)F^{17}$ cross section is also of interest in astrophysics. In hydrogen stars with central temperatures greater than about fifteen million degrees Kelvin, the main energy source is the conversion of protons into alpha particles by means of the

carbon-nitrogen cycle. In this process various isotopes of carbon and nitrogen act as catalysts in the conversion, as follows:

$$\left.\begin{array}{l} C^{12}(p,\gamma)N^{13} \longrightarrow C^{13} + \beta^+ \\ C^{13}(p,\gamma)N^{14} \\ N^{14}(p,\gamma)O^{15} \longrightarrow N^{15} + \beta^+ \\ N^{15}(p,\alpha)C^{12} \end{array}\right\} \quad \begin{array}{l} 4H^1 \longrightarrow He^4 + 2\beta^+ + Q \\ \text{where } Q \simeq 27 \text{ Mev.} \end{array}$$
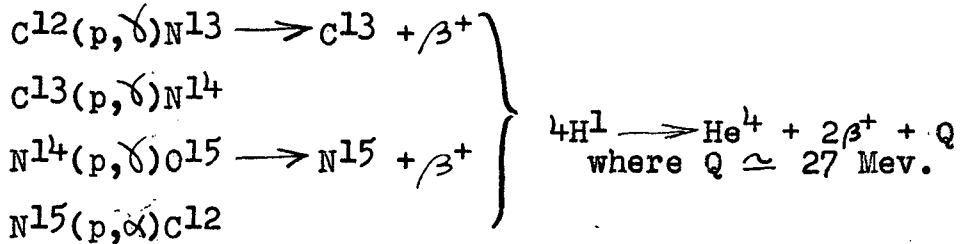
Some of the catalyst is lost from the cycle by the reaction $N^{15}(p,\gamma)O^{16}$. However the reaction $O^{16}(p,\gamma)F^{17}$, followed by $F^{17}(\beta^+)O^{17}$, $O^{17}(p,\alpha)N^{14}$ puts oxygen nuclei back into the cycle. The $O^{16}(p,\gamma)F^{17}$ cross section determines, after a long period, the carbon oxygen ratio in the star as a function of the stellar temperature (Cameron, 57). Since cross section measurements at stellar energies are not accessible to laboratory measurement in this case, theoretical estimates extrapolated from experimental cross sections at higher energies must be used. In order to make this extrapolation with any reasonable accuracy it is necessary that the energy dependence as well as the absolute theoretical cross section be checked experimentally in the high energy region. Previously theoretical calculations by Salpeter (55) and interpretation of experimental results by Laubenstein and Laubenstein (51) assumed that the reaction proceded by compound nucleus formation through the tails of resonances above 4 Mev. and at 0.5 Mev. in F^{17}. However, the results of Warren et al (54) for the $O^{16}(p,\gamma)$ reaction indicate that the reaction proceeds by direct radiative capture of the protons, similar to the $D(p,\gamma)He^3$ reaction.
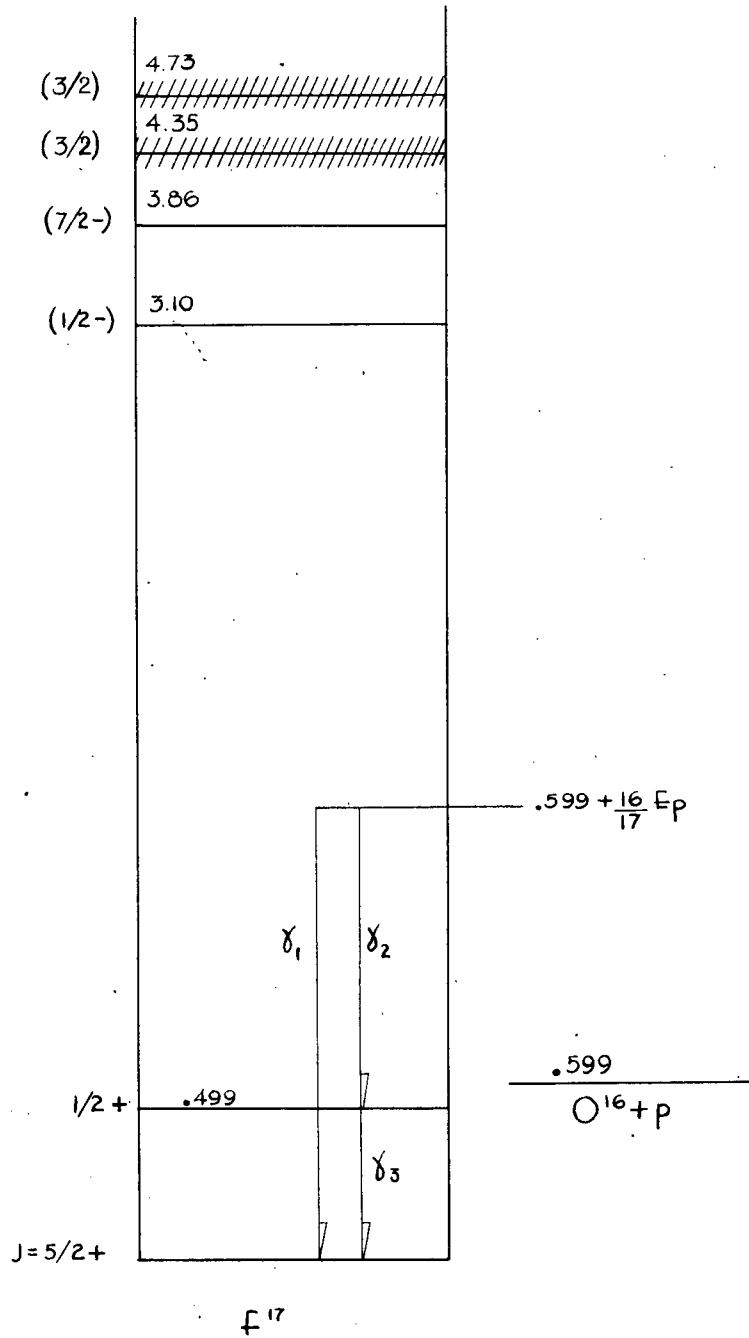
FIGURE 1. F¹⁷ LEVEL SCHEME

In this case the energy dependence of the reaction will differ from that predicted by the compound nucleus assumption.

The $O^{16}(p,\gamma)F^{17}$ reaction was first observed by measuring the annihilation quanta from the decay of F^{17} (DuBridge et al, 38). Laubenstein et al (51) measured the relative cross section as a function of energy from 1.4 to 4.1 Mev. by measuring the yield of annihilation radiation. The relative elastic scattering cross section of protons was also measured from 0.6 to 4.5 Mev. Warren et al (54), in this laboratory, first observed the gamma radiation directly and attributed the non-resonant character of the cross section for gamma emission in the region 0.8 to 2.1 Mev. to a direct radiative capture process and not to the effect of a broad low level nor the resonant levels of higher energy. The $O^{16}(p,\gamma)F^{17}$ cross section was measured at 1.90 Mev. and found to be $6 \pm 3 \times 10^{-30} cm^2$. The low energy levels and spins of F^{17} obtained from previous work are shown in Figure 1. In the work of Warren et al (54), the following gamma rays were observed in addition to the annihilation radiation from the F^{17} positron decay: A ground state transition, γ_1, of energy 16/17 E_p + Q; a transition to an excited state at about 0.5 Mev., γ_2; and the transition from this excited state to the ground state of F^{17}, γ_3. The observed Q value was consistent with 0.594 Mev. deduced from the $O^{16}(d,n)F^{17}$ threshold measurements of Butler (51) at a deuteron energy of 1.631 Mev. (This has been corrected to 1.626 Mev. (Bonner, 55) thus putting the Q at

0.599 $\pm$ .006 Mev.).

Because of the need for a more accurate determination of the absolute cross section to check the theoretical calculations being performed by the California Institute of Technology group, the differential cross section has been measured at 800 kev. in the present work. The gamma ray energies have also been remeasured in order to resolve some of the inconsistency in the literature.

Warren et al (54) observed that gamma radiation of 873 kev. appeared for energies greater than 1.8 Mev. during proton bombardment of oxygen targets. The radiation was attributed to the inelastic proton scattering from the 873 level in O^{17}. During the present work separated targets of O^{16} and O^{17} were bombarded with protons to attempt to confirm this assignment.

CONNECTED TO TARGET CHAMBER

GLASSWOOL

T_1

T_2

T_3

VIAL

H_2O DISPENSER

MANOMETER

LIQUID NITROGEN RESERVOIR

LUCITE

LEAD SHEILDING

LUCITE

ALIGNMENT BELLOWS

ISOLATING VALVE

VAPOUR TRAP

BEAM

1/4" Au STOP

3/8" STOP

3/8" STOP

1/4" Au STOP

1" HOLE IN Cu VAPOUR TRAP

Pt FOIL

Cu BACKING
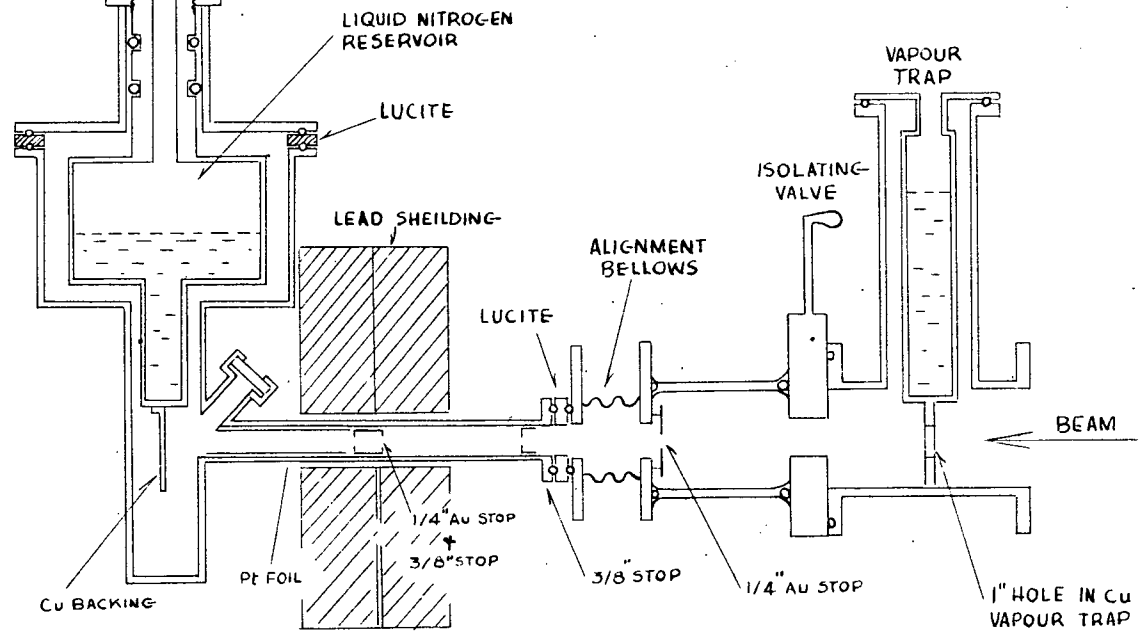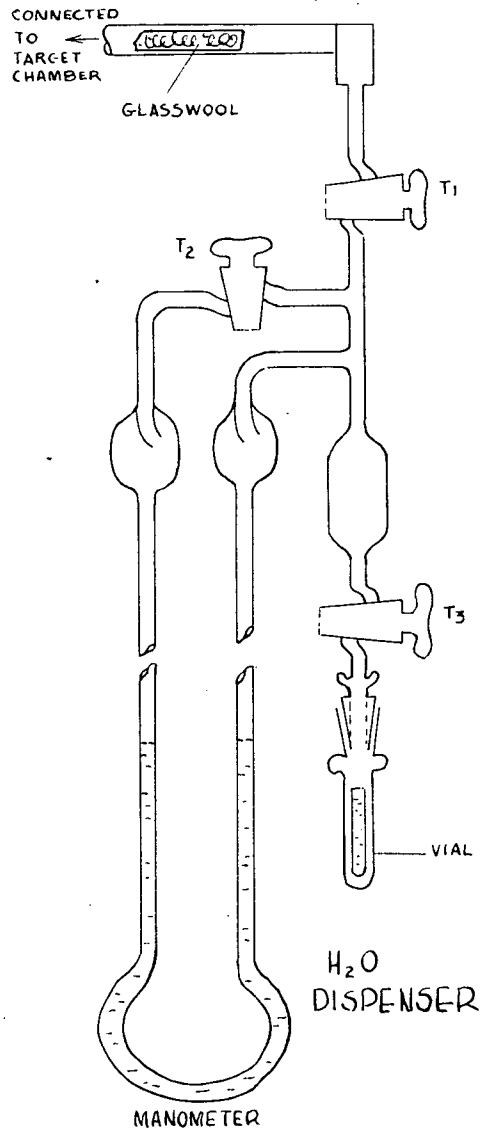
FIGURE 2   TARGET CHAMBER ARRANGEMENT

CHAPTER II
$O^{16}(p,\gamma)F^{17}$ CROSS SECTION MEASUREMENTS

The aim of the present work has been to measure the
cross section of the $O^{16}(p,\gamma)F^{17}$ reaction and the branching
ratio for the two gamma rays from the capturing state to an
accuracy of about ± 10 per cent at 800 kev. proton bombarding
energy, using an ice target whose thickness could be measured
reasonably accurately. 800 kev. was chosen as the bombarding
energy in order to minimize the effect of carbon contamination
and still be able to resolve γ_2 from the 0.51 Mev. annihilation
radiation.

1. **Apparatus.**

    (a) Target Arrangement.

The target was distilled water frozen onto a gold plated
copper backing 1/16 in. thick which was attached to the bottom
of a liquid nitrogen cold trap. The target chamber and stop
arrangement are shown in Figure 2. Since fluorine targets had
been used in the chamber for the target thickness calibrations,
the walls of the chamber in the region of the target were gold
plated with a thickness sufficient to stop 10 Mev. protons. The
stops used, to ensure accurate positioning of the beam on the
target, were gold plated copper to reduce coulomb excited gamma
rays produced by other low atomic number materials (Stelson and
McGowan, 55). The target and support were insulated with a lucite

ring to enable beam current measurements to be made; a positive potential of 135 volts was applied to the target system to reduce secondary electron error in the beam measurement. The beam current was integrated with a current integrator (Edwards, 50). This integrator is essentially a miller integrator circuit whose voltage output is a function of the charge fed onto the integrating condensers. The output of the miller integrator operates a schmidt trigger circuit; the level at which this triggers corresponds to a certain amount of charge on the integrating condensers. Each time this charge is reached it operates a relay which discharges the condensers and drives a mechanical register. Two sets of integrating condensers in parallel permit discharging of one set while maintaining the integration circuit operative. Thus no correction is required for the recovery time of the circuit. The integrator was calibrated by feeding it with a known current supplied from a 100 volt battery. The current was determined by measuring the voltage across a standard resistance with a Rubicon potentiometer. The 100 volt source was required to ensure that the variation in current, due to the 0.5 volt swing on the input of the integrator over each integrating cycle, was small. This measurement indicated that over a one year period the integrator calibration was constant to within one per cent.

(b) Gamma Ray Detector.

A cylindrical sodium iodide, thallium activated (Harshaw) crystal, 2.5 in. diameter by 3.5 in. long, mounted on a Dumont

6363 photomultiplier was used as a gamma ray detector. Dow Corning 200,000 centistokes silicone oil was used as an optical coupling between the crystal and the photomultiplier; a vulcanized rubber sleeve held the photomultiplier and crystal together and prevented the silicone oil from leaking. No noticeable reduction in resolution was noticed over a period of one and a half years. Fitted with a mu-metal shield, the photomultiplier with the crystal was mounted in a 3.5 in. brass tube which also housed the preamplifier.

The efficiency of the large crystal for gamma rays has been measured at 6.14 Mev. and at 1.17 and 1.33 Mev. The 6 Mev. measurement was carried out using the $F^{19}(p,\alpha,\gamma)O^{16}$ reaction at energy 340 kev. (Larson, 57). The method was first suggested by Van Allen and Smith (41). The apparatus used in the present measurements was developed by G.M. Griffiths at the Cavendish Laboratory, Cambridge and the measurements were made by E. Larson and the author and are more fully reported by Larson (57). A thin F^{19} target was bombarded with 340 kev. protons and the α particles were counted in a thin window proportional counter with an accurately known solid angle subtended at the target. Since both the alpha particles and the γ-rays are emitted isotropically and there is one 6.14 Mev. gamma ray for each alpha particle counted, a measurement of the number of alpha particles gives a measure of the number of 6.14 Mev gamma rays simultaneously emitted by the target. A correction must be made for the 2.3 per cent yield of 6.9 and 7.1 Mev. gamma rays for which the cor-

responding alpha particles are not sufficiently energetic to count
in the alpha counter (Dosso, 57). P. Singh and H. Dosso (57)
in this laboratory have measured the efficiency for Co^{60} gamma
rays using a source calibrated by the National Research Council
of Canada. P. Singh has estimated theoretically the efficiency
at this energy and agreement is within experimental errors placed
on the Co^{60} source. The agreement between theoretical calcula-
tions and measured efficiency for 6 Mev. gamma rays is within 5
per cent. Extending the estimates to lower energies is considered
reasonable because of the good agreement in these upper ranges.
A more exact efficiency value in this low region is expected
from pending results in Co^{60} coincidence work.

For 800 kev. proton bombardment of oxygen, the $O^{16}(p,\gamma)$
F^{17} gamma rays, γ_1 and γ_2, have energies of 1.32 and 0.81 Mev.
respectively. The efficiency for gamma rays, $\varepsilon(E, E_b)$, defined
as the ratio of the number of counts of a gamma ray of energy,
E, above a given bias energy, E_b, to the number of gamma rays in-
cident on the crystal, has been obtained for these gamma rays by
considering the theoretical absorption coefficients and the de-
tailed shape of the experimental gamma ray spectra. Since the
detailed shapes of the γ_1 and γ_2 spectra were not accurately ob-
served in the experiment due to the presence of several gamma
rays, additional comparisons were made with the spectra from Na^{22}
and Cs^{137}. The following results relevent to the $O^{16}(p,\gamma)F^{17}$
radiations were obtained; for γ_1 the efficiency is $\varepsilon(1.32, 1.0)$
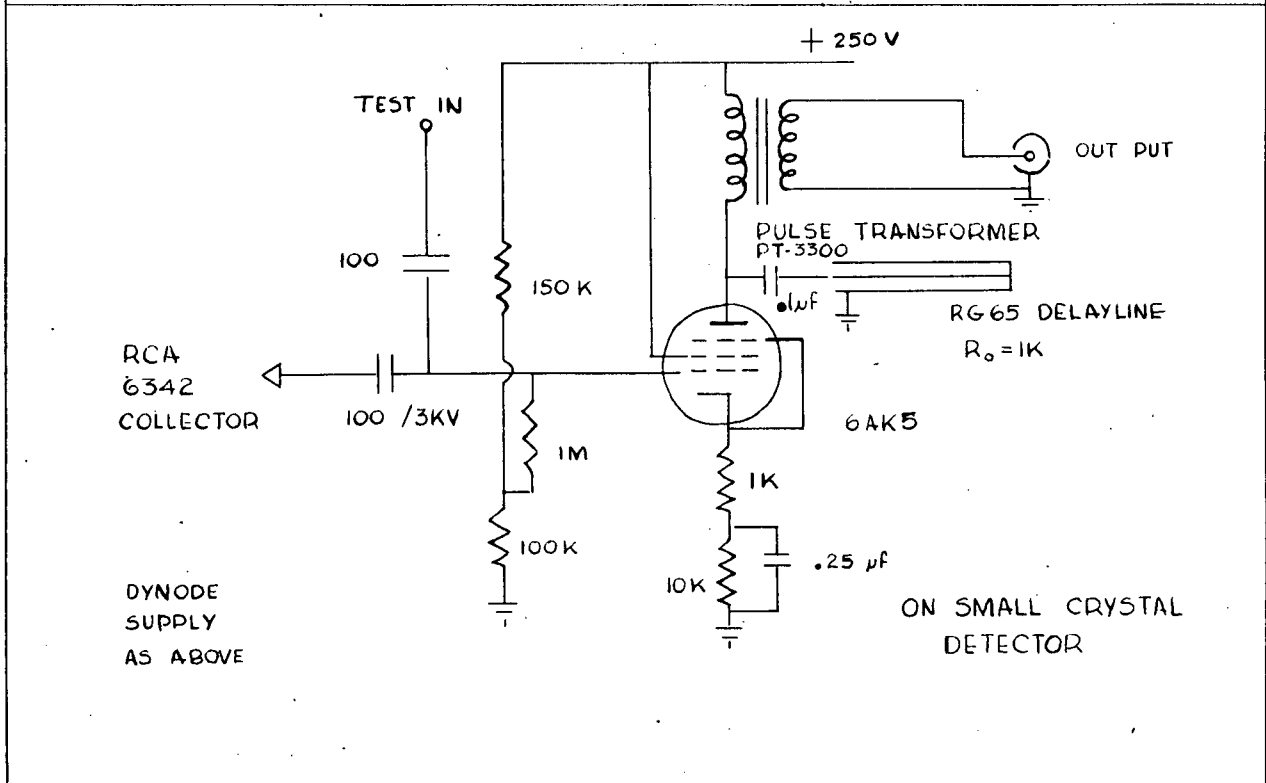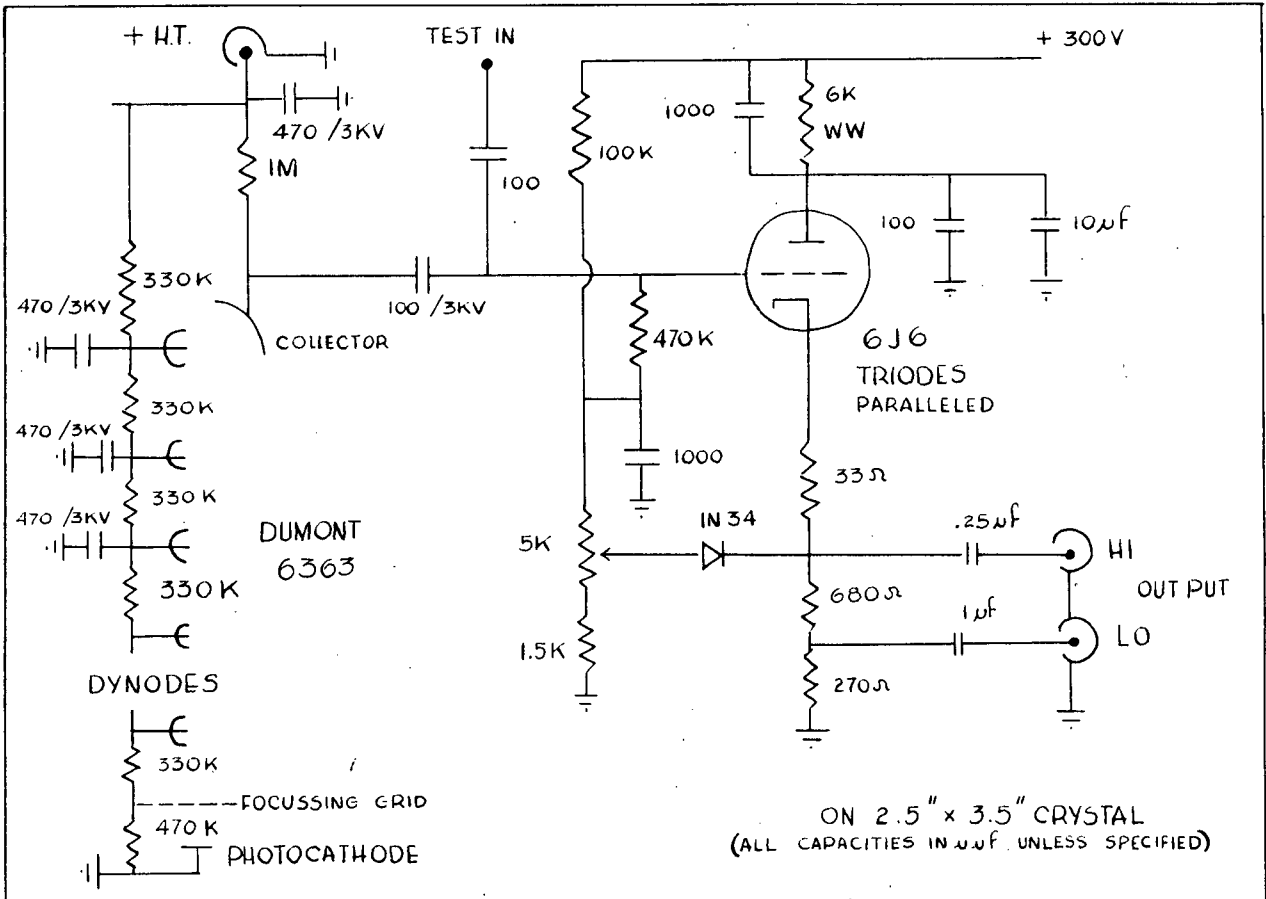
FIGURE 5   PHOTOMULTIPLIER HEAD AMPLIFIER

= (38 ± 5) per cent and for γ_2 the efficiency is ϵ_2(0.81, 0.65) = (31 ± 4) per cent.

A 1.75 in. by 2 in. sodium iodide thallium activated Harshaw crystal was also available, but the larger crystal was used because its efficiency was more accurately known. Also, being larger in area, for a given solid angle the larger coun- ter could be placed further from the target so that errors due to the target to crystal distance measurements and in the po- sitioning of the beam on the target were relatively smaller. Room radiation presented about the same shielding problem to both crystals.

(c) Electronics.

The 1000 volts for the photomultiplier dynode chain was supplied by an Isotopes Development Limited stabilized power supply. A 6J6 cathode follower was used as a preamplifier with a diode clipper to limit the size of large cosmic ray pulses. (Figure 5). The negative pulses from the preamplifier were fed to a Northern Electric wide band amplifier Type 1444 then to a biased amplifier. The output from the biased amplifier was fed to a Marconi 30 channel kicksorter. The kicksorter channel edges were set up by feeding pulses from the mercury pulse generator (Appendix I.) onto the grid of the cathode follower. Then any non-linearity in the components other than the photo-multiplier were compensated for in setting up the kicksorter with the ac- curately linear pulse generator. The pulses fed into the head amplifier also checked the stability of the electronics. The

electronics with the exception of the photomultiplier proved to
be adequately stable.

2. Target Thickness Measurements.

In order to measure the absolute cross section to an
accuracy of about 10 per cent, the number of target nuclei per
square centimeter must be known to an accuracy better than this.
To produce such a target with a known number of oxygen atoms per
square centimeter a system for producing ice layers of repro-
duceable thickness was constructed. A fixed volume of water
vapour whose pressure was measured by an oil manometer was con-
densed onto a cooled copper support attached to a liquid nitro-
gen reservoir. The thickness of the target as a function of
pressure of water vapour in the dispenser was determined in terms
of the energy loss of 340 kev. protons in passing through the
ice layer. This was found by measuring the centroid shift of
the 340 kev. $F^{19}(p,\alpha,\gamma)$ resonance when the ice layer was con-
densed on a thin fluorine target. The dispensing system was cal-
ibrated for heavy water, however the calibration applies equally
well to ordinary water since the number of molecules of gas con-
tained in the dispenser for a given pressure is the same for both
gasses. Negligible differences could have resulted from the
difference in the heat of fusion and the Van der Waal's constant
of the two gases. Using the values of the molecular stopping
cross section for heavy water measured experimentally by Wenzel
and Whaling (52) the number of ice molecules per square centimeter

as a function of manometer pressure can be determined from measurements of the energy loss of protons in passing through the ice layer for targets corresponding to several different manometer readings.

The dispenser, Figure 2, was made of glass with glass taps ground to give a vacuum tight fit. Octoil Vacuum Pump Oil, (vapour pressure 10^{-7} mm. at 20°C, density 0.9 gm. per c.c.) heated under vacuum to remove high vapour pressure impurities, was used in the manometer. The fluorine targets were prepared by evaporating calcium fluoride onto cleaned copper sheets (Larson, 57); these were indium soldered onto a 1/16 in. thick copper support attached to the liquid nitrogen reservoir.

In order to make a reproduceable target the following procedure was adopted. The manometer was evacuated to the side arm pressure with taps T_1 and T_2 open. See Figure 2. With T_1 and T_2 closed, T_3 was opened until the desired pressure of water vapour was reached and T_3 was closed. When equilibrium was established in the manometer, the temperature of the air and the manometer reading were recorded. The target assembly was rotated so that the cooled copper plate faced the outlet of the dispenser. Tap T_1 was opened carefully to leak the water slowly into the target chamber and the manometer read again when the water had been expelled from the dispenser. T_1 was then closed. The side arm pressure measured at the magnet box was approximately 10^{-6} mm. of mercury. If the pressure rose higher than

Protons on Fluorine

Protons on Fluorine With Ice Layer

Counting Rate

Proton Energy
KEV.
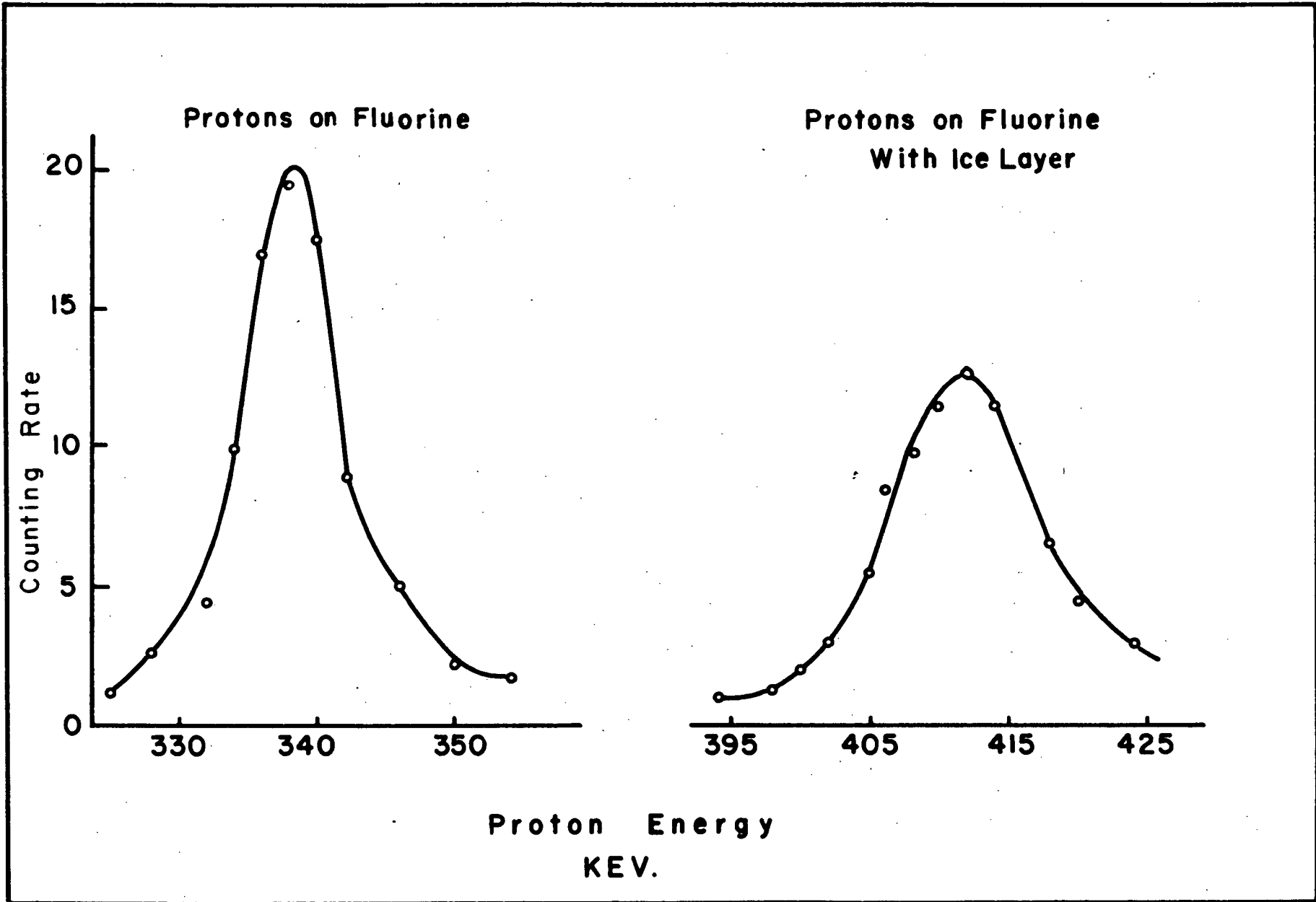
Fig. 3 - D$_2$O Ice Target Thickness Calibration

10^{-5} mm. due to leaks, the reproduceability in target thickness was considerably reduced and the thickness measured for manometer readings of 10 - 20 cm. of oil was lower. The vapour pressure of water at 20°C corresponded to a manometer reading of 24 cm. By using pressures of water less than the vapour pressure, errors due to condensation on the walls of the dispenser were reduced.

The linearity and absolute calibration of the Van de Graaff energy scale measured by the generating voltmeter were determined by noting the positions of the 0.224, 0.340, 0.480 and the 0.669 Mev. resonances of $F^{19}(p,\alpha,\gamma)O^{16}$.

Figure 3 shows the centroid shift of the 340 kev. resonance. An ice layer corresponding to a water pressure of 13.6 cm. of oil was layed down on the fluorine target. The increased width of the resonance for the target with the ice layer is due to the non-uniformity of the target which amounts to about 10 kev. Proton beams of 0.5 microamperes were used during these calibration runs. Currents higher than 1 microampere caused deterioration of the targets which appeared as a broadening of the resonance curve. Since the position of the centroid did not shift with bombardment and the area under the resonance curve remained constant the broadening was attributed to a decrease in the uniformity of the target and not to either a reduction in the mean heavy ice thickness or a deterioration of the fluoride target.
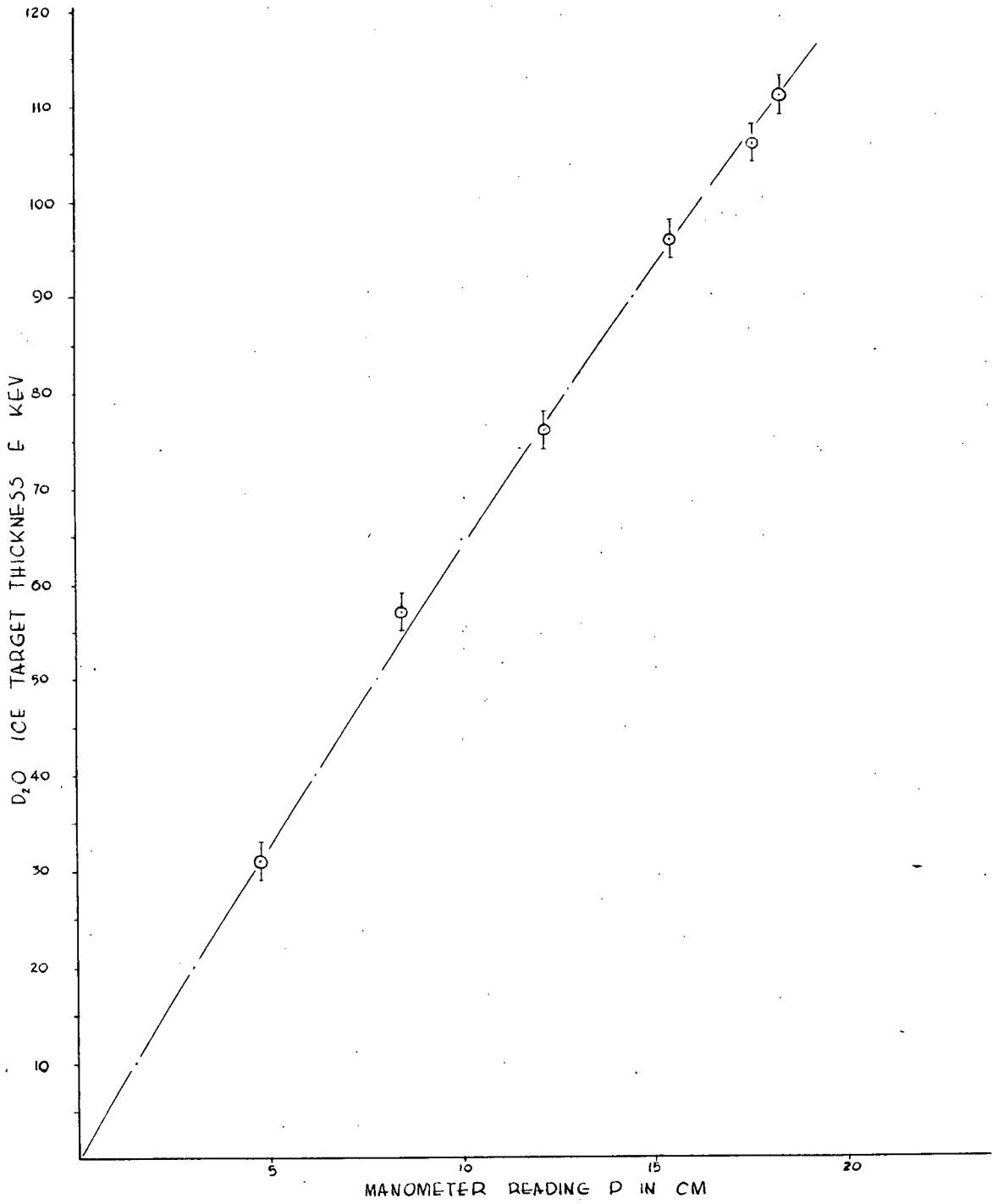
FIGURE 4 D_2O DISPENSER CALIBRATION

The results of the measured energy loss of protons in the ice targets as a function of the manometer reading, P, are shown in Figure 4. To determine from this data the number of heavy ice molecules per square centimeter on the target a knowledge of the molecular stopping cross section at these energies is required. Wenzel and Whaling (52) have measured the molecular stopping power, σ_{D_2O}, of heavy water as a function of energy. They indicate that their results agree to within experimental error with the theoretical values calculated by Hirschfelder and Magee (48) using the semi-empirical theory of Bethe (37) for the stopping power. Whaling (57) has collected data for hydrogen and oxygen and for water which give slighly higher values than the experimental measurements on heavy water for the proton energy range 300 to 500 kev. In this work the measured stopping cross sections of Wenzel and Whaling were used for the calculation of the number of molecules per square centimeter.

The molecular stopping cross section as a function of proton energy, E, in the region from 340 kev. to 460 kev. can be approximated by $\sigma(E) = A + B(E)$ where $E = E' - 340$ kev. and E' is the bombarding energy. This function was fitted to the experimental curve given in Wenzel and Whaling (51) at 360 and 430 kev., with the result that

$$\sigma = (14.9 - 0.0238\ E)\ 10^{-15}\ \text{ev.-cm.}/ \text{ molecule of } D_2O.$$

Now the molecular stopping cross section is defined as $- \dfrac{1}{N}\dfrac{dE}{dx}$

where N is the number of molecules per cubic centimeter. Then $\int_0^x dx = -b \int_0^E \frac{dE}{\sigma}$ where E is the total energy loss for protons passing through a distance x of heavy water and b is a constant. Assuming that the thickness of ice is proportional to the dispenser manometer reading, then $P = \frac{1}{c} \int_0^E \frac{dE}{\sigma}$ where c is a proportionality constant. Substituting for σ

$$P = \frac{1}{c} \int_0^E \frac{dE}{A + BE}$$

$$= \frac{1}{cB} \ln \left(1 + \frac{B}{A} E\right)$$

$$E = \frac{A}{B} \left(e^{cBP} - 1\right)$$

This function is plotted in Figure 4 for the case of CB = -0.0107, chosen to fit the experimental points. From this curve one can determine the water target thickness in kev. for protons in the energy region just above 340 kev. With this and the molecular stopping cross section for heavy water (Wenzel and Whaling, 52) the number of molecules per cubic centimeter, nD_2O, was obtained.

$$nD_2O = \frac{T \times 10^3}{\sigma}$$

where T is the target thickness in kev, σ is the molecular stopping power for $E_p = 340 + T/2$ in ev.-cm^2/molecule.

Ice targets for the oxygen cross section measurements were made using distilled water from the U.B.C. Chemistry Department.

3. Experimental.

(a) Background.

Accurate measurement of gamma yields become increasingly difficult the lower the gamma energy because the background rises quickly with decreasing energy below about 2 Mev. The background in this region is due to secondary cosmic radiation, radiation from natural radioactive salts in the concrete (K^{40} 1.4 Mev., RdTh 2.62 Mev.), reactions due to contaminants in the target, and machine X-ray background. Since these are relatively low energy radiations, approximately 4 in. of lead is sufficient to reduce this background to a reasonable level. When running at 800 kev. machine energy, however, the counter must be shielded on all sides to reduce radiation from the room. Therefore, 4 in. of lead was placed around the counter and the target chamber so that none of the room was visible to the counter. With the arrangement used the time dependent counting rate was 60 counts per minute in the energy range 0.5 to 3 Mev.

Lead and paraffin blocks were placed between the magnet box and the counter to reduce background from the (d,n) reactions in the magnet box.

Proton bombardment of carbon contamination on the target produced 2.37 Mev. gamma rays from $C^{12}(p,\gamma)N^{13}$ and annihila-

tion radiation from the subsequent positron decay of the N^{13}.
The assignment of the gamma ray to C^{12} was consistent with the
energy measurement of $2.36 \pm .04$ Mev. and the position of a reso-
nance for this gamma ray at 460 kev. Some of the carbon contam-
ination was present in the gold plated backing but the largest
source was from the hydrocarbon pump oils and vacuum greases used
in the vacuum system which condensed on the cold target plate.
Prior to laying down a target the target chamber was baked at
$150^{\circ}C$ for 24 hours to reduce the amount of oils which condensed
on the cold target during the runs. Because of the presence of
the C^{12} contamination, it was decided not to measure an absolute
cross section at higher energies with the ice target but to make
a relative cross section measurement as a function of proton
energy using a stable oxide target which could be heated to pre-
vent carbon deposition. Then a comparison of the yields at 800
kev. proton energy from the ice target of known thickness and
from the oxide target, would determine the oxide target thickness.
This work has not yet been completed.

(b) Procedure.

Protons of 830 kev. produced by the U.B.C. Van de Graaff
generator were used to bombard two different ice targets. The
beam energy measured by the generating voltmeter and analyzed by
the 90° deflection magnet was known to within about ± 3 kev. With
one target, measurements were made at three different distances
to determine any correction to the solid angle due to the fact
that the angular distribution of γ_2 was not isotropic but of the
form $a(b + \sin^2\theta)$. The target was positioned at 45° to the beam
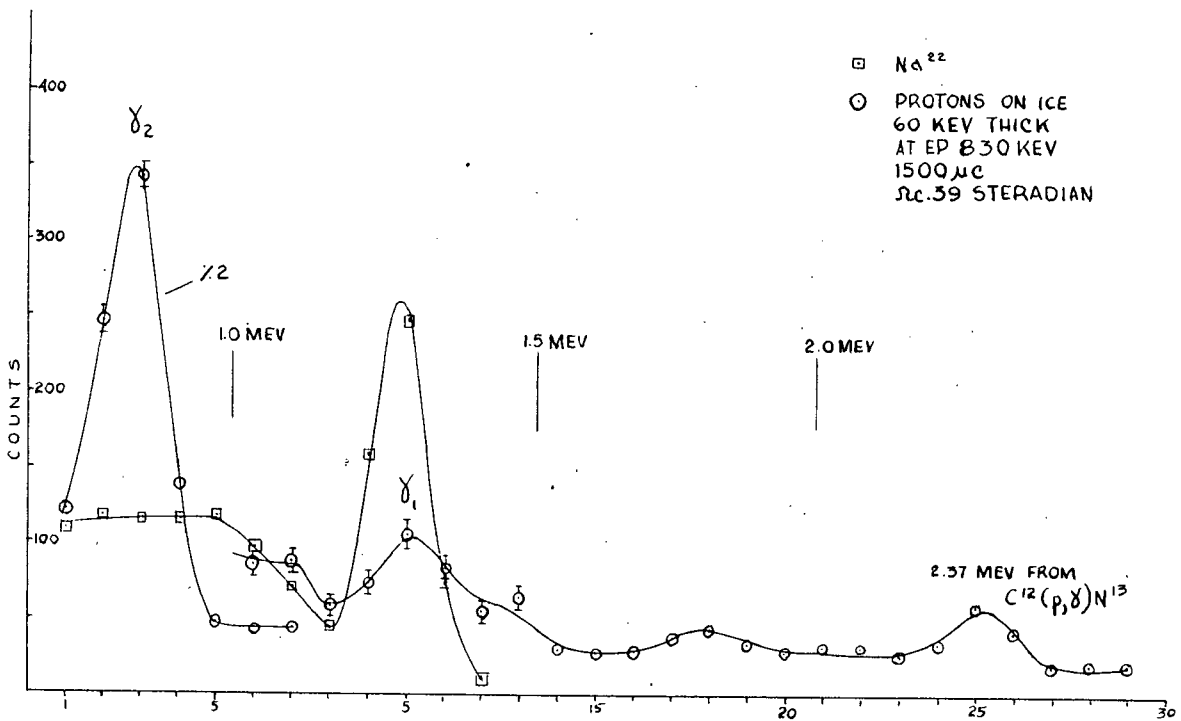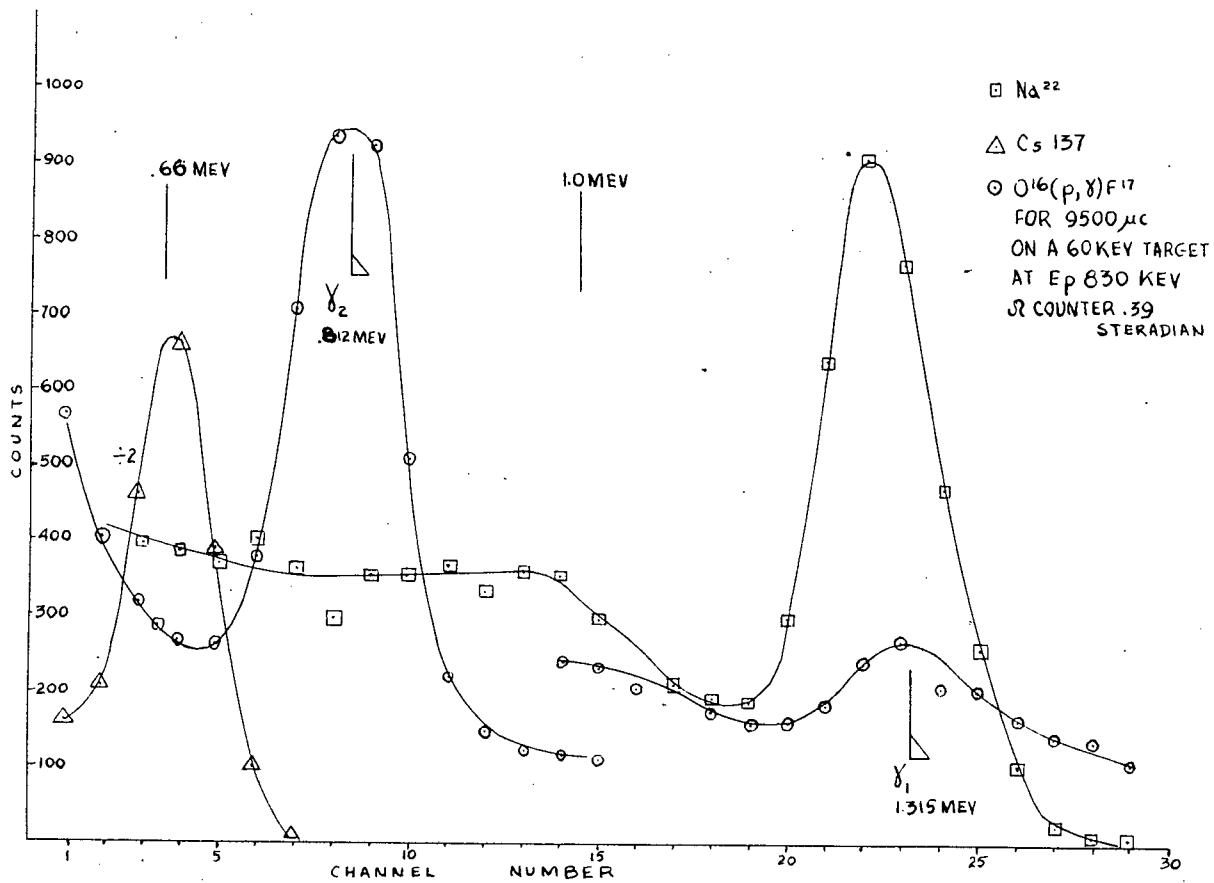
FIGURE 6   SPECTRA FROM ICE TARGETS

after laying down the ice so that the radiation was not attenuated by the copper support. The angular position of the target was obtained from a degree circle attached to the target chamber. The error in angular positioning was $\pm$ 0.5 giving a probable error of $\pm$ 1 per cent in the number of atoms per square centimeter seen by the beam due to uncertainty in target orientation.

Beams of 4 to 5 microamperes of protons were used. The beam was defocussed so that the stop system defined the size and position of the beam spot. No deterioration of the target was observed even after being subjected to total beams of 10^4 microcoulombs other than for the build up of some carbon on the surface.

Spectra were recorded which included γ_1 and γ_2 and also γ_1, γ_2 and the 2.37 Mev. radiation from $C^{12}(p,\gamma)$. This permitted the background due to carbon contamination, which increased in thickness with the amount of bombardment, to be estimated. Periodic checks of the channel positions of the kicksorter for each spectral range showed the electronics were stable to better than 0.5 per cent.

(c) Measurement of the effective centre at 0.51 and 1.28 Mev.

A knowledge of the effective centre position for the gamma ray energies measured was required. Since the gamma rays are absorbed throughout the 3.5 in. long detector crystal, measurements of the counting rate will not show an inverse square dependence on the distance measured from a source to the end of the

FIGURE 7   EFFECTIVE   CENTRE
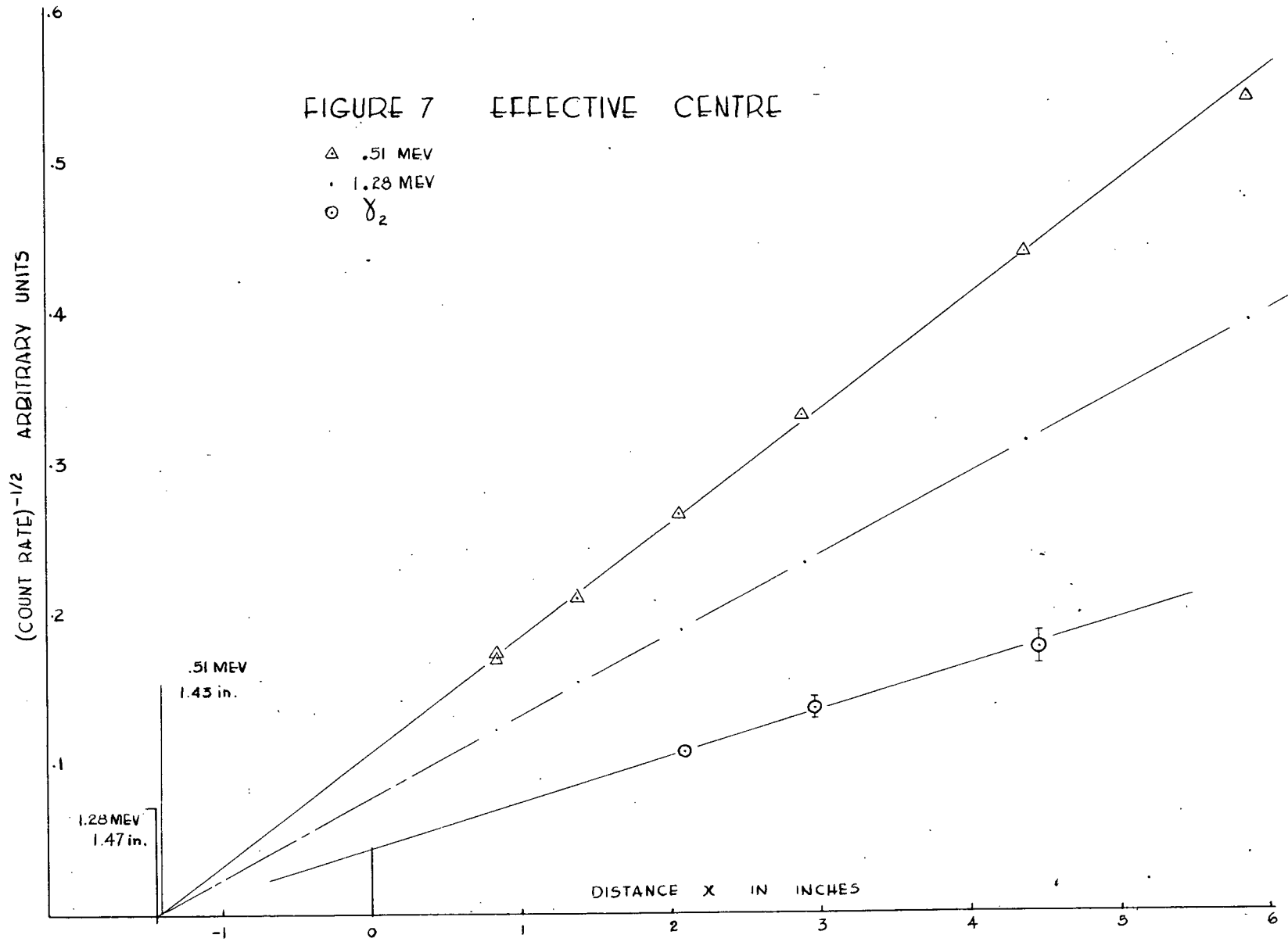
crystal. However experimentally it has been shown that if distance measurements are made from the source to a point inside the crystal which we call the effective centre the inverse square relation between counting rate and distance will hold, except for distances of the same order as the crystal dimensions. This point can be thought of as the mean distance inside the crystal at which absorption takes place. This permits one to define an efficiency which is independent of distance. Also the theoretical efficiency calculated for plane incident gamma ray fluxes will correspond to this definition of efficiency. The distance to the effective centre depends on the gamma ray energy since the absorption coefficient is energy dependent. The effective centre was determined experimentally for gamma ray energies close to those obtained in the $O^{16}(p,\gamma)F^{17}$ reaction by using a Na^{22} source and measuring the counting rate as a function of distance from the end of the crystal for both the 0.51 Mev. and the 1.28 Mev. gamma rays. A Na^{22} source contained in a 0.25 in. diameter aluminum rod was placed in the target chamber at the position where the beam struck the ice target and the counting rate of the 0.51 and 1.28 Mev. gamma rays for different counter to source distances were measured. The results are shown in Figure 7. From the straight line fitted by least squares, the distances from the crystal face to the effective centre for 0.51 and 1.28 Mev. radiations were $1.432 \pm .08$ in. and $1.47 \pm .10$ in. respectively. These are to be compared to the $1.60 \pm .10$ in. found for the effective centre distance at 6.14

Mev. To within the probable error the effective centre distance
for the three energies are the same.

An estimate of the effective centre position may be
made assuming that this is the distance, x, from the front face
of the crystal such that half the total absorption takes place
in front of x (assuming a plane incident flux and neglecting
multiple processes and losses through the crystal sides). Then
$x = - \frac{\ln (0.5 (1 + \exp -\mu \ell))}{\mu}$, where μ is the total absorption

coefficient, and ℓ is the length of the crystal. The ratios
$x_{6.14}$: $x_{1.28}$: $x_{0.51}$ are 1: 0.6: 0.45 which differ from those
measured experimentally. This difference has not been accounted
for and further measurements are needed to determine the cause of
the discrepancy.

4. Cross Section Calculations.

   (a) Carbon Contamination Correction.

     Since the number of 2.37 Mev. gamma rays from $C^{12}(p,\gamma)N^{13}$
depends on the duration of the bombardment, and because much of
this contamination evaporated at the same time that the target
was allowed to evaporate, beam dependent backgrounds taken with
no ice on the target did not give a true measure of the C^{12} back-
ground effect. Therefore, in making background corrections the
following procedure was adopted. First, the beam dependent
background was subtracted under each of the peaks (from 0.652 to
0.995 Mev. in the case of γ_2, and from 0.995 to 1.45 Mev. in the
case of γ_1). In the case where the spectra included the C^{12} γ-rays

the background was also subtracted from the 2.37 Mev. peak. The residue in the spectrum between 1.45 and 2.5 Mev. with beam and time dependent background subtracted was assumed to be due to C^{12} build up during the run. On the basis of the 2.37 Mev. gamma ray spectrum shape, an amount proportional to this residue was subtracted from the γ_1 and γ_2 regions of the spectrum. The proportions subtracted were estimated from a C^{12} spectrum taken previously during contamination checks. This C^{12} correction was significant in the case of γ_1 but not in the case of γ_2 which had a much higher yield.

(b) Solid Angle

From runs taken at three counter distances on one of the ice targets the counts per integrator for γ_2 followed an inverse square plot as a function of the distance to the effective centre measured for the .51 Mev. gamma rays to better than 3 per cent. This indicates that the solid angle subtended by the counter during the cross section measurements is sufficiently small that the $\sin^2\theta$ component of γ_2 does not significantly affect the calculation of the cross section if constant flux per unit solid angle is assumed. Integrating a $\sin^2\theta$ yield over the counter area at the effective centre for the distance used above gives a result differing by the order of 3 per cent from that of an isotopic distribution.

(c) Calculation of cross section

The series of runs taken on each target were summed and the cross section estimated for the two cases separately and then compared. The calculations for one of the targets are given below.

The differential cross section is defined by:

$$\frac{d\sigma}{d\Omega_{\gamma_i}} = \frac{1}{\alpha_i} \frac{N\gamma_i}{(\mathcal{E}_i A)} \cdot r^2 \cdot \frac{1}{n_p} \cdot \frac{1}{n_O}$$

where $\mathcal{E}_i A$ is the efficiency times area of the face of the counter

ter r is the target to effective centre distance

   n_p is the number of protons incident on the target

   α_i is the transmission coefficient through the 1/16 inch brass walls which is .916 for .8 Mev., .935 for 1.3 Mev. gamma rays

   n_O is the number of O^{16} atoms per square centimeter

With a manometer reading of 18.75 centimeters of oil for the target used, the corresponding thickness of D_2O was 107 kev to 390 kev protons as read from the calibration curve Figure 4. The stopping cross section per D_2O molecule for protons of this energy as given by Wenzel and Whaling (52) is $\sigma_{D_2O} = 13.5$ x 10^{-15} ev-cm^2. Therefore, the number of oxygen atoms of mass 16 per centimeter seen by the beam, including a $\sqrt{2}$ factor since the target was at $45°$ to the beam, is given by

$$n_O = f \cdot \frac{107 \times 10^3}{13.5 \times 10^{-15}} \times \sqrt{2}$$

$$= 1.118 \times 10^{19} \text{ atoms per cm}^2$$

where f is relative natural abundance of $O^{16} = .9976$

$$n_p = \frac{95 \text{ integrator counts} \times 107.2 \text{ microcoulombs}}{1.602 \times 10^{-13}}$$

r = 3.54 inches

$N_{\gamma 2}$ = 7982 counts above a bias of 1.0 Mev., after background corrections

A = 4.909 in.^{2}

$$\left(\frac{d\sigma}{d\Omega}\right)_{\gamma_1} 90^\circ \cdot \mathcal{E}_2 = \frac{7982}{.916} \times \frac{(3.54)^2}{4.909} \times \frac{1.602 \times 10^{-13}}{95 \times 107.2} \times \frac{1}{1.118 \times 10^{19}}$$

$$= 3.15 \times 10^{-32} \text{ centimeters}^2 \text{ per steradian}$$

Putting in the efficiency of 31 per cent this gives the differential cross section

$$\left(\frac{d\sigma}{d\Omega}\right)_{\gamma_1} 90^\circ = 10.2 \times 10^{-32} \text{ cm}^2 \text{ per steradian.}$$

The ratio of the relative yields at 90 degrees of γ_1 and γ_2 is calculated as follows:

$$\frac{\left(\frac{d\sigma}{d\Omega}\right)_{\gamma_1}}{\left(\frac{d\sigma}{d\Omega}\right)_{\gamma_2}} \Bigg/ _{\Theta = 90^\circ} = \frac{N_{\gamma_1}}{\mathcal{E}_1} \cdot \frac{\mathcal{E}_2}{N_{\gamma_2}} \cdot \frac{\alpha_2}{\alpha_1}$$

$$= .1751 \cdot \frac{\mathcal{E}_2}{\mathcal{E}_1} \cdot \frac{.916}{.935}$$

Putting in the efficiencies .38 for $\mathcal{E}_1$ and .31 for $\mathcal{E}_2$ we get the ratio of the number of γ_1 to γ_2 observed at 90 degrees as 0.14.

(d) Errors

The sources of error in the differential cross section measurement of γ_2 are tabulated below.

Source		Probable Error	Probable Error in Cross Section Measurement
n_O	calibration of dispenser	1.5%	±4.5%
	σ_{D_2O}	4%	
	Angular position of target	1%	
r	effective centre and beam position	±.02% ±.05%	±2%
ε_1		±12%	
ε_2		±12%	12%

The probable error in the number of counts from γ_2 per intergrator count estimated from the consistency between the runs on a given target give ± 2% for the 107 kev. target and ± 3.7 per cent for the 93 kev. target in reasonable agreement with the statistics on the gamma-ray counts in each run.

The probable error in the ratio of the cross sections for γ_1 and γ_2 calculated from the consistancy of the ratio of $N\gamma_1$ to $N\gamma_2$ for all runs is ±1.3 per cent. With the error of 17 per cent in the ratio ε_1 to ε_2, this gives a resulting probable error of 17 per cent in the ratio of the differential cross sections.

5. Results.

The differential cross section was measured using protons of incident energy 830 ± 5 kev.

Since the protons lose energy in traversing the ice target the mean proton energy at which the reaction occurs is a better indication at what energy the reaction was measured. Assuming the $O^{16}(p\gamma)F^{17}$ cross section is relatively constant for protons of energy over the range appearing in the target, then $\overline{E}p = Ep + \dfrac{\Delta}{2}$ where Ep is the incident proton energy in kev. and Δ is the target thickness in kev. For the targets used in the cross section measurement the thickness was approximately 60 kev. for 800 kev. protons; therefore $\overline{E}p = 800 \pm 10$ kev.

The results of the measurements on the two different ice targets gave the differential cross section at 90 degrees of γ_2 as $(10.4 \pm 1.3) \times 10^{-32}$ cm^2 per steradian.

Using the angular distribution of γ_2 found by Warren et al (55) as being proportional to $1 + 5 \sin^2\theta$ at 1.9 Mev. for the angular distribution at 800 kev., the total yield for γ_2 integrated over all angles is given by:

$$\sigma_{t_2} = \frac{4\pi (1+2/3 \times 5)}{6} \times \left(\frac{d\sigma_2}{d\Omega}\right)_{90^\circ}$$

$$\therefore \sigma_{t_2} = 9.3 \times 10^{-31} \text{ cm}^2 \text{ for } \gamma_2 \text{ at 800 kev.}$$

The relative differential cross section at 90 degrees of γ_1 to γ_2 is 0.14 ± 0.03

The total relative yields, again using the angular distribution for γ_2 at 1.90 Mev is given by

$$\frac{\sigma_{t1}}{\sigma_{t2}} \quad \frac{6}{1 + 2/3.5} \quad x\ 0.14 + 0.19$$

From this and the value for σ_{t2}, σ_{t1} is 1.8×10^{-31} cm.^{2}

The intensity ratio of γ_1 to γ_2 is significantly higher than .1 found previously in this lab at 1.90 Mev. However before these results can be accurately compared with the earlier work, angular distributions at 800 kev. need to be measured.

CHAPTER III
ENERGY DETERMINATION OF γ_3

1. Introduction.

The measurement of the gamma ray energy from the excited level at approximately 0.5 Mev. in O^{16} is of interest because of discrepancies between various previous measurements of this energy. A knowledge of the position of this level is necessary for the calculations of the cross section at low energies. Also results differing greatly by different methods of measurement indicate that either the accuracy of some methods are not as good as supposed or the level structure is more complex than believed.

The level energy was first measured by F.A. Ajzenberg (51) for the reaction $O^{16}(d,n)$. The neutron angular distribution was measured by photographic plate technique. From the energy separation of the two neutron groups the level was placed at 536 ± 10 kev. Previous work done in this laboratory (Warren et al) indicated that the level was less than 0.51 Mev. above the ground state by direct measurement of the energy of γ_3. The energy was estimated to be 487 ± 15 kev. Preliminary unpublished work by Bonner agreed more closely with Ajzenberg (Ajzenberg and Lauritsen, 55). However, as a result of more accurate measurement of the threshold for $Li^7(p,n)Be^7$, Bonner and Marion (55) measured the energy as 499 ± 3 kev. again using $O^{16}(d,n)$ thresholds,

confirming the estimates obtained in this laboratory. The threshold neutrons were detected by making fast-slow neutron ratio measurements as a function of deuteron energy, with an estimated probable error of $\pm$ 0.006 kev. Doyle et al (56) using the N^{14} (α,n)F^{17} reaction give 0.53 $\pm$ 0.04 Mev. as the level energy; the high probable error would support either of the previous determinations, not only Ajzenberg's results as indicated by Doyle.

The determination of the energy of γ_3 was repeated, because of this latest report, and to check that the earlier results obtained were reproduceable.

2. <u>Apparatus</u>.

(a) Target.

Because of the difficulty in shielding the counter and target system with lead when the ice dispenser was used and in reducing carbon contamination on the cold target support, it was decided to use solid oxidized metal targets.

Tungsten was used because of the low energy of the coulomb excited states at 112 kev. (Stelson and McGowan, 55). K X-rays (66 kev. for tungsten) and bremstrahlung would be present with all materials used; tin has negligible coulomb excitation but is difficult to oxidize. A tungsten plate 0.020 in. by 1 in. by 0.75 in. was cleaned in potassium hydroxide (20 per cent solution) etched, and rinsed thoroughly with distilled water. The tungsten was oxidized by suspending it in a heater coil of

nickel wire inside a bell jar, heating the strip under vacuum and admitting cylinder oxygen (commercial grade). The tungsten surface discoloured green, bright blue and then blue-gray as the oxide layer thickened. A long period of heating in an atmosphere of oxygen produced a yellow-green surface due to the formation of tungsten trioxide. This changed back to the blue-gray colour where the beam hit it during bombardment presumable due to the tungsten trioxide changing back to tungsten dioxide. Therefore for a target with a constant oxygen content, the blue-gray tungsten dioxide layer was preferable.

Since bombardment of sodium gives a 0.45 Mev. gamma ray from $Na^{23}(p,p')$, as well as a 1.60 Mev. gamma ray for $Na^{23}(p,\alpha,\gamma)Ne^{20}$, the target was checked for Na^{23} contamination by running an excitation curve over the resonances at 1287.5 and 1257.5 kev. The resonance at 1257.5 kev. decays mostly by proton emission giving the 0.45 Mev. gamma ray. Traces of Na^{23} were apparent. From the excitation function for $Na^{23}(p,\alpha,\gamma)$ and $Na^{23}(p,p',\gamma)$ given by Stelsen and Preston (54) for proton energies greater than 1 Mev. and by R.L. Burling (41)for protons from 0.3 to 1.9 Mev., the Na^{23} yield was estimated to be less than 10 counts per 100 microcoulombs of beam above a 300 kev. bias for 830 kev. proton energy for the counter-target geometry used during the measurement of γ_3. This residual Na^{23} effect was sufficiently small that it would produce negligible distortion of the γ_3 peak.

The target chamber used was similar to that used by Alexander (55). Steam heat was applied to the target assembly to reduce the amount of oil vapours condensing on the target. During some bombardments no steam was used and no typical cracked oil deposit appeared on the target. It therefore appears that if the vacuum system is clean the heating of the target by the beam along with good cold trapping close to the target assembly are sufficient to prevent oil vapour contamination of the target.

A lead shield was moulded to fit the geometry of the target chamber and fit into the lead castle housing the gamma ray counter.

(b) Detector and Electronics.

The large 2.5 in. by 3.5 in cylindrical Harshaw sodium iodide thallium activated crystal was used as a detector, positioned to touch the chamber face thus subtending approximately 0.015 of a sphere at the target.

The kicksorter was set up as described in Chapter II. The stability of the electronics during the runs was better than 0.1 per cent as measured by the mercury pulse generator. The full energy peaks of the gamma rays were measured with a high dispersion of the kicksorter to afford maximum energy resolution.

3. Experimental.

(a) γ_1 and γ_2.

Protons with an energy of 800 kev. as read on the generating voltmeter were used to bombard the oxide target positioned
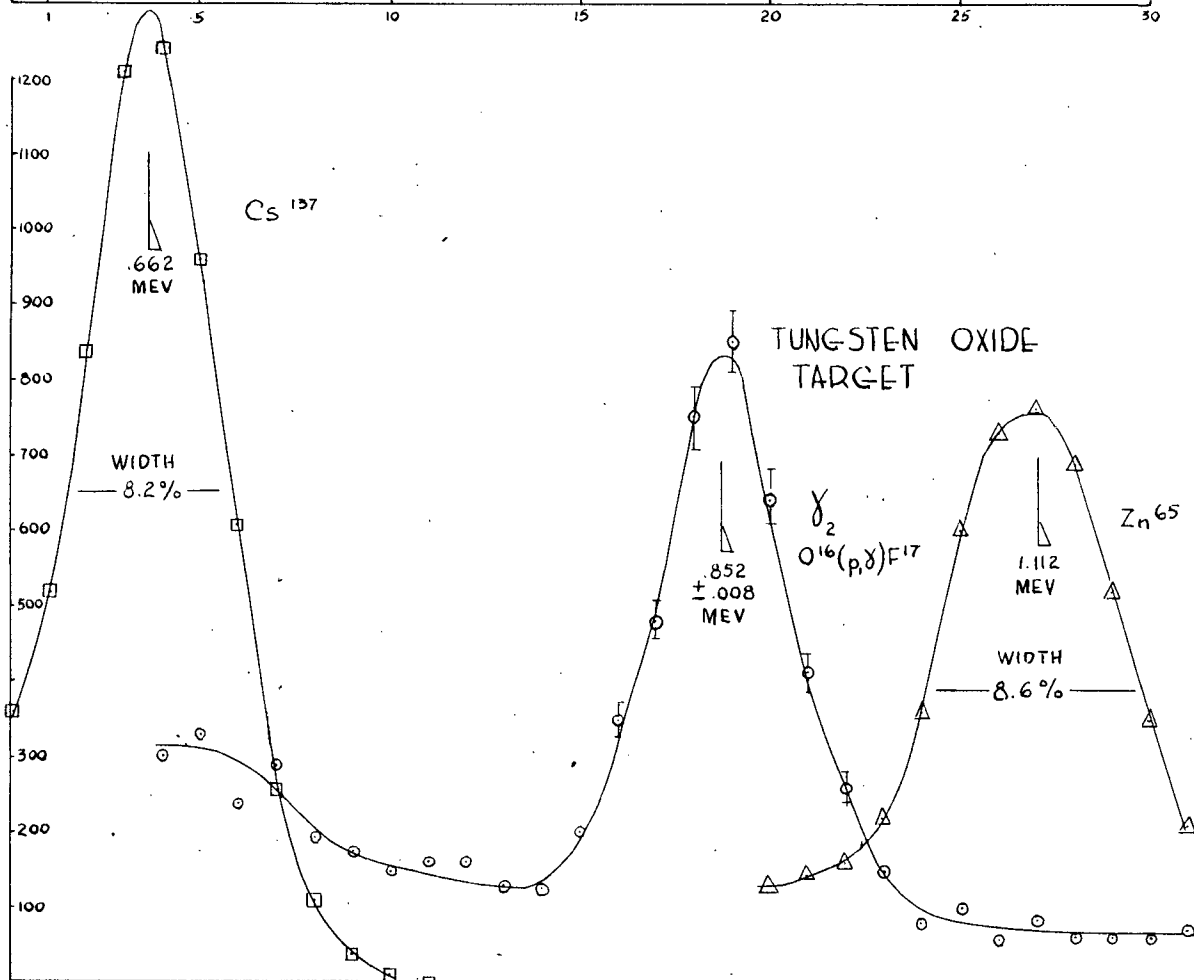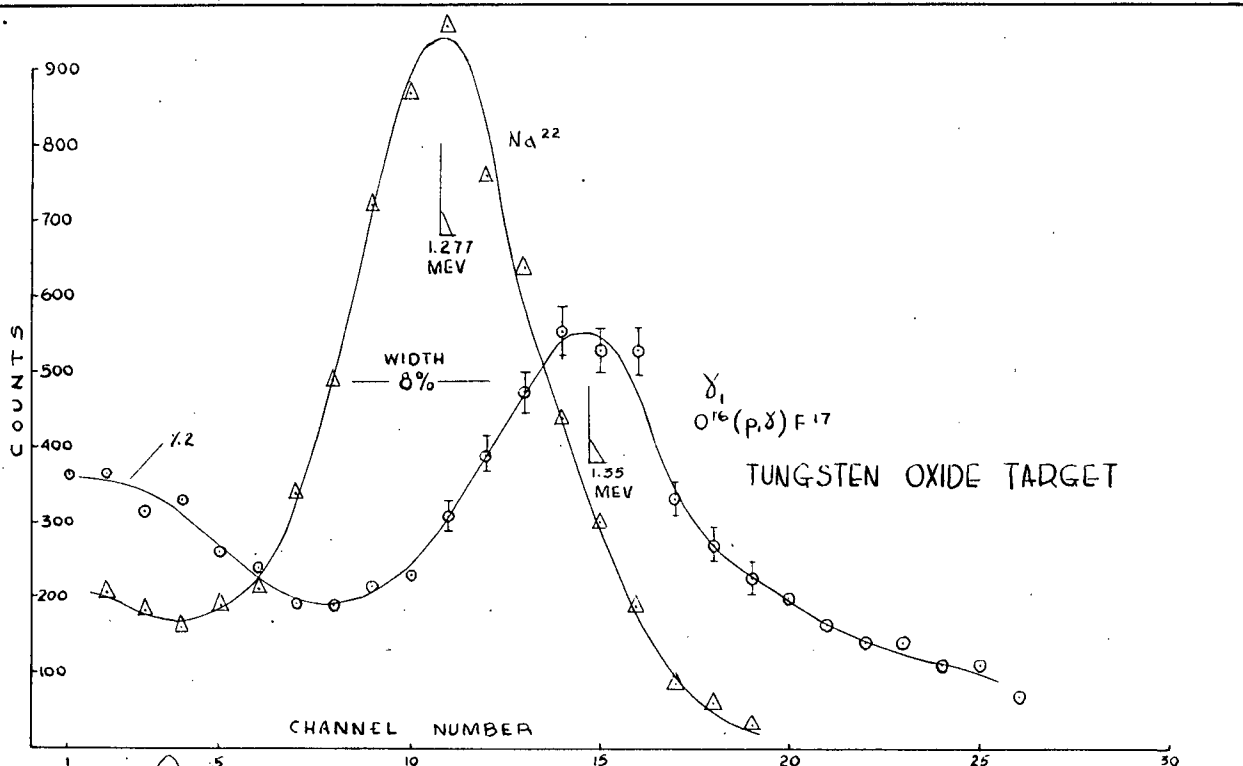
FIGURE 8   O^{16}(p,γ)F^{17} GAMMA RAY ENERGIES

so that the gamma rays were not attenuated by the target support
in the direction of the detector. The 1.12 Mev. gamma ray from
Zn^{65}, the 0.662 Mev. gamma ray from Cs^{137} and the 1.28 Mev.
gamma ray from Na^{22} supplied calibration points for the pulse
generator amplitude scale. The linearity of the crystal pulse
height versus gamma ray energy was better than 1 per cent in
this region.

The curves used to determine the energies of γ_1 and γ_2
are shown in Figure 8.
The results of these measurements indicate

$$E_{\gamma_1} = 1.346 \pm 0.018 \text{ Mev.}$$

$$E_{\gamma_2} = 0.852 \pm 0.008 \text{ Mev.}$$

$$E_{\gamma_1} - E_{\gamma_2} = 0.494 \pm 0.012 \text{ Mev.}$$

The generating voltmeter was calibrated at the 873.5 kev. reso-
nance of $F^{19}(p,\alpha,\gamma)$ on a thin fluorine target.

The Q value for the reaction may be determined from γ_1
and E_p.

$$Q = E_{\gamma_1} - \frac{16}{17} E_p \qquad\qquad 1$$

Because the protons lose energy as they traverse the target a mean
proton energy, E_p, must be used and since the reaction is non-
resonant, $\overline{E_p} = E_p - \Delta/2$, where Δ is the target thickness (expressed
in kev.) to protons of energy E_p. An estimate of the number of O^{16}

atoms per square centimeter can be made from the relative yield of γ_2 on the tungsten dioxide target as compared with that on the ice target of known thickness. The energy loss in the tungsten dioxide target will then be given by,

$$\Delta_E = \sigma_{WO_2} \cdot \eta_0 \cdot \tfrac{1}{2} \, ,$$

where σ_{WO_2} is the molecular stopping power for tungsten dioxide,

η_0 is the number of O^{16} atoms per square centimeter and $\tfrac{1}{2}$ accounts for the fact that there are two oxygen atoms per molecule.

σ_{WO_2} may be calculated from atomic stopping power data given by Whaling (57) as follows:

$$\sigma_{WO_2} = \sigma_W + 2\,\sigma_0.$$

Since Whaling does not give σ_W, extrapolation from σ_{Au} assuming $\sigma \propto Z$ can be used to get σ_W

Then $\sigma_{WO_2} = \dfrac{74}{79}\ \sigma_{Au} + 2\,\sigma_0$

$$= 35.0 \times 10^{-15} \text{ e.v.-cm}^2/ \text{ molecule at } E_p = 0.800 \text{ Mev.}$$

The number of counts in the full energy peak of γ_2 for the oxide target with the detector 2.3 in. from the target was 62 counts per integrator. With the same detector set at 3.6 in. from an ice target of thickness $\eta_{H_2O} = 1.118 \times 10^{19}$ molecules of water per square centimeter, there were 92 counts per integrator in the γ_2 full energy peak. The number of oxygen atoms per

square centimeter on the oxide target was calculated as follows

$$\eta_0 = \frac{N\gamma \text{ oxide}}{N\gamma \text{ ice}} \cdot \frac{\Omega \text{ ice}}{\Omega \text{ oxide}} \cdot \eta_{H_2O}$$

where $N\gamma$ is the number of gamma rays per integrator, and Ω are the solid angles for the two cases

$$\eta_0 = \frac{62}{92} \times \left(\frac{2.3}{3.6}\right)^2 \times 1.118 \times 10^{19} \text{ atoms/cm}^2$$

Then the energy loss for protons passing through the tungsten dioxide is

$$(\Delta_E)_{WO_2} = 35.0 \times 10^{-15} \times \frac{1}{2} \times \frac{62}{92} \times \left(\frac{2.3}{3.6}\right)^2 \times 1.118 \times 10^{19}$$

$$(\Delta_E)_{WO_2} = 53 \pm 10 \text{ kev.}$$

This result assumed that the oxygen was in the form of WO_2. The target surface was blue-brown in colour characteristic of the dioxide rather than the yellow colour of the trioxide. If some WO_3 was present this would reduce the target thickness.

A 53 kev. thick target should have resulted in an increase in the observed widths of γ_1 and γ_2 by approximately 50 kev. The observed increase in the widths is less than 10 kev. The inconsistency of the two results is rather puzzling and is not yet explained. Assuming that tungsten trioxide is formed, $(\Delta E)_{WO_3}$ = 38 kev., still rather wider than can be accounted for by the width of the observed gamma ray lines. Assuming (ΔE) = 53 kev.

to be correct then for an incident proton energy E_p = 831 kev. the mean proton energy on the target $\overline{E_p}$ = 804 kev. For E_{γ_2} = 1.346 Mev. from Equation 1 we obtain Q = 590 $\pm$ 23 kev. This agrees within experimental error with the value 0.599 $\pm$ .006 Mev. calculated from the $O^{16}(d,n)F^{17}$ threshold (Bonner and Marion, 55).

It is interesting to compare the above results on gamma ray energies with similar results obtained from the ice targets below:

$$E_{\gamma_1} = 1.315 \pm .016 \text{ Mev.}$$

$$E_{\gamma_2} = .812 \pm .016$$

$$E_{\gamma_1} - E_{\gamma_2} = .503 \pm .032 \text{ Mev.}$$

To determine the Q value from γ_1, the target thickness at an incident proton energy of 830 kev. must be calculated in order to estimate the mean proton energy.

The ice targets were 100 kev. thick for 390 kev. protons; this corresponds to a thickness of 60 kev. at 800 kev., calculated using 0.6 for the ratio of the molecular stopping cross sections for water at 390 and at 830 kev. (Whaling 57). Then E_p = 800 kev. $\pm$ 10 kev. and Q = 562 $\pm$26 kev. The Q here is lower than would be expected from the known mass values.

The spreading of the proton energy due to the target thickness will produce a spread in the energy of γ_1 and γ_2. The widths of the full energy peaks of γ_2 and γ_1 are about 40 $\pm$ 15

kev. greater than the widths of the full energy peaks of the
.661 Mev.γ-ray of Cs^{137} and the 1.28 Mev. γ-ray of Na^{22} respec-
tively. Since the target thickness was calculated to be 60
kev., the measured width of the $O^{16}(p,\gamma)F^{17}$ gamma rays should be
60 kev. wider than that due to the resolution of the detecting
system. This is greater than the measured value, however just
outside the error placed on the measured width increase.

If the cross section is falling rapidly with decreasing
energy in this region of bombarding energy, the width increase
would be correspondingly reduced since there is a relatively
larger yield in the front portions of the target compared with
the back portion where the reactions are produced by lower energy
protons. This would help explain the lack of observed increase
in the tungsten oxide targets. However it seems rather unlikely
that the radiative captive cross section would change so rapidly
over this small energy range at 800 kev. Also the effect should
be observable equally on the tungsten oxide target as on the ice
target since the energy loss for protons in the two targets was
approximately the same. Another reason why results from the
tungsten oxide target do not show as large a broadening of the
full energy peaks as expected assuming all the oxygen is in the
form of tungsten oxide is that some oxygen may be occluded as a
surface layer on the tungsten so that the relative energy loss
of the protons due to the tungsten atoms is reduced; for a pure
oxygen target of such thickness to give an equivalent yield as
measured, the energy loss for 800 kev. protons would be approximately
10 kev.

Also it should be mentioned that for this crystal mounted on the Dumont 6363 photomultiplier the width of a full energy peak of the 1.28 Mev gamma ray of Na^{22} varied as much as 20 per cent amongst sets of runs taken under approximately the same conditions. This variation in the resolution although not accompanied by gain shifts of the centroid, reduces greatly the information available from the width of a peak in a gamma ray spectrum.

(b) Energy determination of γ_3

Since the energy of γ_3 is very close to the 0.51 Mev. annihilation radiation from the positron decay of F^{17} which is also produced in the reaction, the resulting spectrum will be due to the sum of the appropriate number of gamma rays of the two energies. The shape of the resulting spectrum and the position of the maximum of the curve will depend on the resolution of the detector, the difference in energy between the two gamma rays, and the relative intensity of the gamma rays.

Assuming the full energy peak due to a single gamma ray is gaussian in shape, the spectrum shape for a gamma ray whose energy width is very small compared to the resolution of the detector may be described by the usual gaussian equation

$$\frac{dN(x)}{dx} = \frac{N}{2\pi\sigma} e^{-1/2\frac{(x-\mu)^2}{\sigma^2}} \qquad 2$$

where σ is the half width at .606 peak height.

.51 MEV SPECTRUM
WITH .49 MEV SPECTRUM
INTENSITY RATIO 2:1

$\delta = 16$ KEV.
$\sigma = 28$ KEV.

11%
RESOLUTION

⊙ ANNIHILATION RADIATION
SPECTRUM FROM Na²²

COUNTS

POSITION OF Na²² ANNIHILATION
PEAK.

FIGURE 9

γ_3 ENERGY
MEASUREMENT

.4 MEV   .5 MEV

max.

⊙ FIRST MINUTE
   BOMBARDMENT (i)

△ EQUILIBRIUM (ii)

⊡ F¹⁷ ANNIHILATION
   RADIATION (BEAM OFF)(iii)

COUNTS

CHANNEL NUMBER
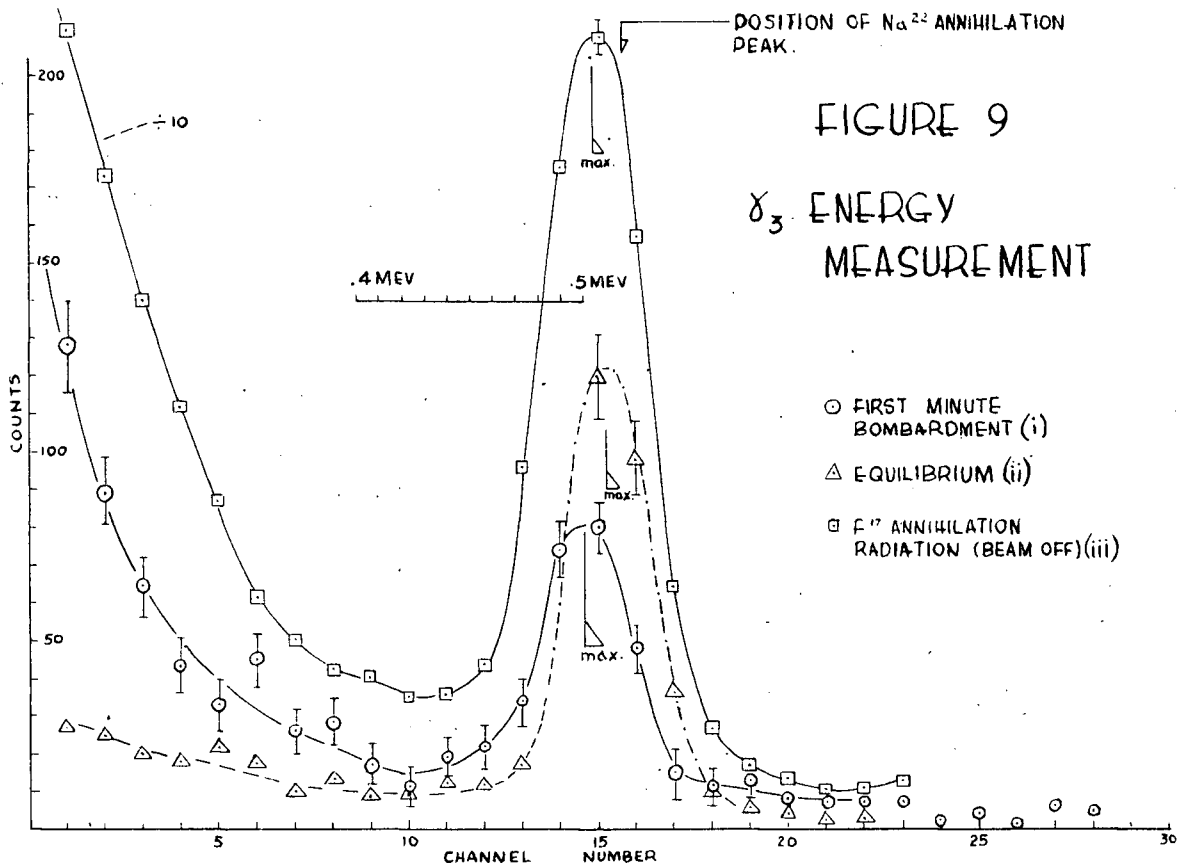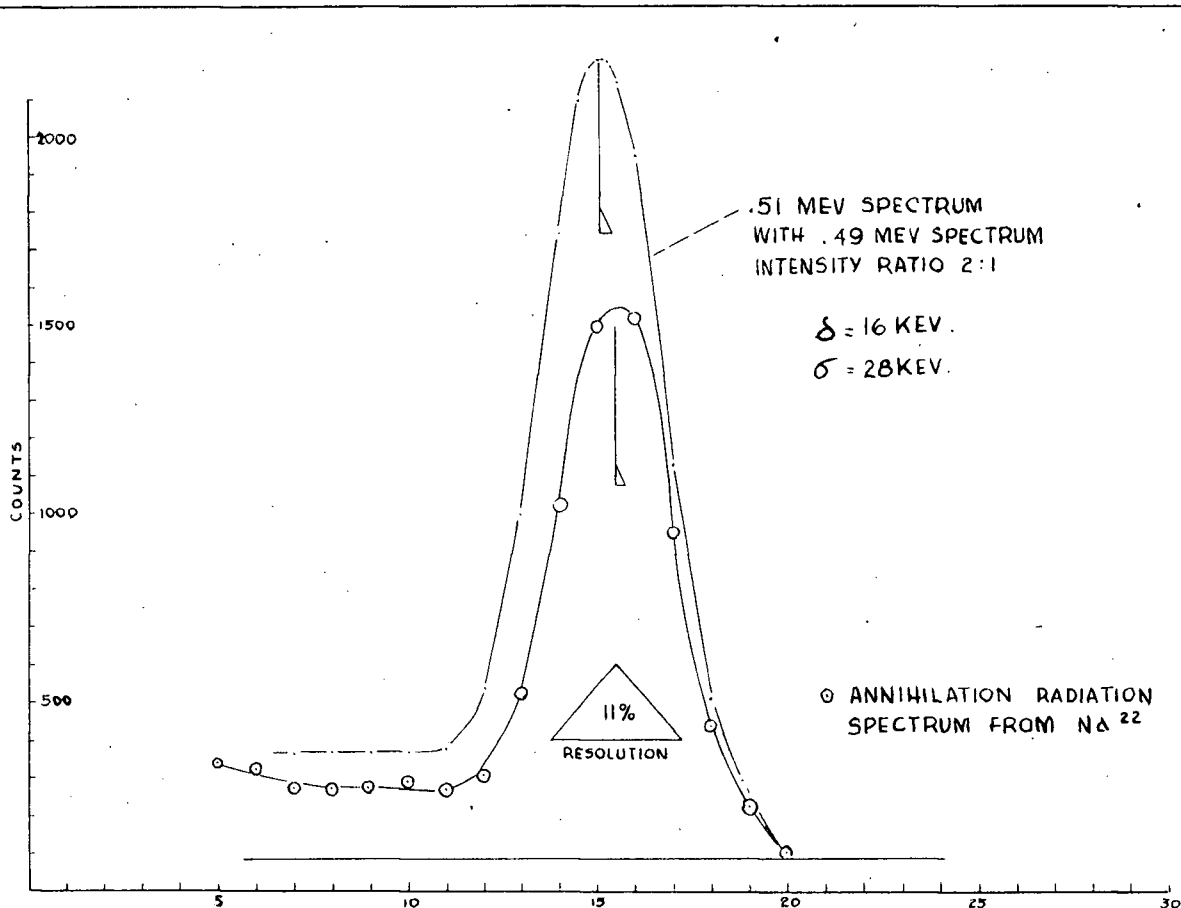
(the width at half peak height is

$$\Delta_{\frac{1}{2}} = 2\sigma(\ln 4)^{1/2})$$

x is the pulse height in volts

μ is the centroid of the distribution

N is the total number of counts in the peak

Two gamma rays whose energies are close together, i.e. within the resolution of the detector, will produce a shape which can be approximated by the sum of two gaussian functions. Therefore to determine how the maximum for such a measured spectrum varies as a function of energy separation and intensity ratios of the gamma rays, we consider the sum of two gaussians:

$$y = \frac{c}{2\pi\sigma}\left(\exp -1/2\frac{(x-\mu_1)^2}{\sigma^2} + r\cdot\exp -1/2\frac{(x-\mu_2)^2}{\sigma^2}\right) \quad 3$$

This represents two gaussians of the same width, one with centroid at μ_1 and area c, the second with centroid at μ_2 and area rc. (Figure 9).

Solving for the maximum, μ_0, of this curve

$$\frac{\mu_0-\mu_1}{\mu_0-\mu_2} = -r\exp\left[\frac{1}{2\sigma^2}\left\{2\mu_0-(\mu_1+\mu_2)\right\}(\mu_2-\mu_1)\right]$$

Let $\delta = \mu_2-\mu_1$

Then $\mu_0-\mu_1 = -(\mu_0-\mu_1-\delta)\,r\,\exp\left[\frac{\delta}{\sigma^2}(\mu_0-\mu_1-\frac{\delta}{2})\right]$

Considering the first order in i.e. $\frac{\delta}{\sigma}\cdot\frac{\mu_0-\mu_1-\delta/2}{\sigma}\ll 1$

Then

$$\mu_0-\mu_1 = \mu_1 r - \mu_0 r + r\cdot\delta$$

$$\therefore \mu_0 = \mu_1 + \frac{r\cdot\delta}{1+r} \qquad 4$$

This result can be used to determine the position of the maximum, Eo, of a complex gamma ray spectrum, of two gamma rays of full energy E_1 and E_2, where $E_2 = E_1 + \delta$, and the intensities are in the ratio 1 to r with a detector resolution such that δ is less than the width of a monenergetic spectrum at .606 peak height.

Then the position of the maximum of the composite spectrum Eo is given by

$$E_0 = E_1 + \frac{r\,\delta}{1+r} \qquad\qquad 5$$

$$\text{for} \quad \frac{\delta}{\sigma} < 1$$

The difference in the width at half maximum between E_1 and E_2 is negligible for these separations.

The width at .606 maximum of a curve of the form of equation 2 is most easily obtained graphically. Figure 9. shows the result of adding two full energy peaks from a Na^{22} spectrum in the crystal, one placed at 0.51 Mev., the other moved to 0.493 Mev. with an intensity ratio of .5. The maximum is shifted $0.4 \pm .1$ of the gamma ray shift; the shift estimated from equation 5 is 0.33, in reasonable agreement. With these considerations in mind we may analyse the spectrum from $O^{16}(p,\gamma)F^{17}$ in the region of 0.5 Mev. gamma ray energy.

* - 39 -

The F^{17} nucleus produced by the $O^{16}(p,\gamma)$ reaction

decays by positron emission with a half life of 66 seconds

(Ajzenberg and Lauritsen (55). The number of γ_3 gamma rays pro-

duced can be calculated from the branching ratio "a" for γ_1 to γ_2:

$$N\gamma_3 = \frac{1}{1+a} N_F$$

where N_F is the number of F^{17} nuclei produced by the reaction.

The number of annihilation gamma rays is approximately

equal to twice the number of F^{17} nuclei which decay during the

counting period.

To estimate the number of F^{17} atoms which decay in a

given period consider the equation which gives the _total_ rate of

change of F^{17} atoms.

$$\left(\frac{d\,N_F}{dt}\right)_{total} = -\lambda\,N_F + ci$$

where ci is the rate of production of F^{17} nuclei which is propor-

tional to the beam current i and which we will assume to be con-

stant; at t = 0, N_F = 0. The number of F^{17} decaying is equal to

$-\lambda N_F$ whereas the number γ_3 being produced is proportional to

the proton current.

The ratio, r, of the number of counts from γ_3 to the

number from annihilation radiation can be determined for the time

intervals below.

a)   o to t

$$r = \frac{c_i \cdot t \cdot \frac{1}{1+a}}{2\int_0^t -\lambda N_F dt}$$ 6

$$r = \frac{1}{2(1+a)} \cdot \frac{t}{(t-T(1-\exp-t/T)}$$

where $T = \frac{1}{\lambda}$ = 95 second, the mean lifetime.

b)   for the time interval t measured at least 5 half lives after starting the bombardment

$$r = \frac{1}{2(1+a)}$$ 7

In figure 9 curve (i) was taken during the first 63 seconds of beam bombardment of the target. Curve (ii) was obtained with a constant beam of approximately $(10^{\pm}.5)$ microamperes bombarding the target for approximately 8 minutes (that is, approximately 5 life times) after which the spectrum was recorded for 10.2 minutes keeping the beam constant during this time. The equilibrium spectrum taken for the first 66 seconds after the beam was shut off is shown in curve (iii).

Estimation of the energy difference between the 0.51 Mev. gamma ray and γ_3 was made as follows:

From curve (i)

Since the halflife of F^{17} is 66 seconds (Ajzenberg and Lauritsen (55)), then t is approximately equal to the half life.

The ratio $\frac{\gamma_1}{\gamma_2}$ as measured above was 0.2. Substituting these values into equation 6 gives r = 4/3. The measured shift is then (8.5 ± 5.2) kev. Therefore from equation 5

$$\delta = \frac{1 + 4/3}{4/3} \times 8.5$$

$$\delta = -15 \text{ kev.} \pm 12 \text{ kev.}$$

From curve (ii)

With a = 4/3, equation 7 gives r = .42. The measured shift is (5.2 ± 5.2) kev. from the .51 Mev. line. This gives δ = -18 kev. ±18 kev. The weighted mean for δ is then -16±12 kev. thus $E_{\gamma_3} = 495 \pm 12$ kev.

(c) Gain Shifts

The difference in the position of the annihilation radiation recorded immediately after the beam was off the target and that from Na[22] (Figure 9) recorded a few minutes later indicates a gain shift in the detection system.

Since the counting rate during the runs in the region about 400 kev. was low (less than 22 counts per second) the gain shift was thought to occur due to the high counting rate from coulomb excited gamma rays from tungsten of 112 kev. and 66 kev. tungsten X-rays as well as the small contribution due to bremstrahlung. A test was run to reproduce this shift. The lack of d.c. shift in the electronics (not including the photomultiplier) was established by putting the mercury popper pulses into the head amplifier and recording these pulses on the K.S. When a Cs[137] source was placed up to the crystal so that the counting

rate was greater than 1500 counts per second above 200 kev., the change in the popper pulse height on the kicksorter was less than .1 per cent.

Eu^{155} gives among other gamma rays strong lines at 330 and 87 kev.; therefore this source with Na^{22} were used to approximate the counting conditions occuring during the runs on the tungsten oxide targets. The counting rate above a 50 kev. bias was increased from 100 counts per second to 1500 counts per second by moving the Eu^{155} source closer to the crystal. During these runs no shift was noticed in the centroid of the 0.51 Mev. full energy peak from Na^{22}. However, on removing the Eu^{155} source the 0.51 Mev. radiation showed a gain shift of +8 kev. approximately equal to that observed between the annihilation radiation from the target and Na^{22} during the bombardment of the oxide.

One explanation of this behaviour would be to assume that there existed two gain shift affects in the photomultiplier with high counting rates in the low energy region of the spectrum (less than 100 kev.) with different decay time constants; one a positive shift which had a long decay time of the order of a few hours, the other a negative shift which had a short decay time of the order of a minute. These affects cancelled each other with a large low energy counting rate, but the gain increase would be observed when the low energy counting rate was reduced.

4. Results.

Summarizing the different measurements of $E\gamma_3$

Target	Measurement	Result
ice	$E\gamma_1 - E\gamma_2$	$.503 \pm .032$ Mev.
WO_2	$E\gamma_1 - E\gamma_2$	$.494 \pm .012$ Mev.
WO_2	Centroid shifts	$.495 \pm .012$ Mev.

The mean of these results is $0.50 \pm .01$ Mev. in agreement with $.499-.003$ Mev. given by Bonner and Marion (55), and within the probable error of the previous results from this laboratory (Warren et al, 54).

CHAPTER IV
A LOOK FOR $O^{17}(p,\gamma)F^{18}$ GAMMA RAYS

1. Introduction.

        According to the shell model the mass 18 nuclei con-
sist of two nucleons outside the closed O^{16} core. Because of
this relatively simple assumptions are possible for the deter-
mination of wave functions for the ground state and some of the
excited states. Elliot and Flowers (54) have calculated the
positions of the low lying levels of the mass 18 and 19 systems
of an intermediate coupling shell model of the nucleus. In or-
der to check the validity of the theory, experimental values of
the spin, parity and isotopic spin of the excited states of F^{18}
are of interest at the present time. A study of the $O^{17}(p,\gamma)F^{18}$
reaction will supply some of the parameters of the F^{18} states
which can be compared to theoretical predictions. Since a sep-
arated O^{17} target was available, it was decided to look for gamma
radiation from this reaction in the region 1.0 Mev. to 2.2 Mev.
proton energy leading to excited states in F^{18} between 6.5 and
7.7 Mev.

        Warren et al (54) found the existence of an 873 kev
gamma ray during the bombardment of natural oxygen targets with
protons of energy greater than 1.8 Mev. This was attributed to
gamma de-excitation of the 872 kev. level in O^{17}(Ajzenberg and

Lauritsen ,55) excited by inelastic scattering of protons. In order to check this assignment, separated targets of O^{16} and O^{17} were bombarded with protons in the energy region around 2 Mev.

From the results, no capture gamma rays from O^{17} could positively be identified. The limit of detectability was set by contaminants. The spectra of capture gamma rays from the contaminants were studied and the results are reported on briefly here as it is felt that they should be useful in connection with further low cross section studies in this energy region.

2. Experimental Procedure.

(a) Gamma Ray Detection Systems

The large 2.5 by 3.5 inch thallium activated sodium iodide crystal was used with the same electronics as described in Chapter III. A gain shift phenomenon was observed on the Dumont 6363 which was a function of the counting rate, the spectrum shape and the H.T. voltage on the dynode chain. The gain tended to increase when the detector was exposed to a high counting rate and did not return immediately to its original value on decreasing the count rate, but slowly dropped over a period of a few hours or more. The amount of the shift was much greater for comparable counting rates above a fixed bias when caused by high energy gamma rays contributing to the fast counting rate than when due to low energy gamma rays. Also the amount of gain shift for a given counting rate and a given spectrum was decreased for lower photomultiplier H.T. voltage. In all cases the

gain of the system was independent of pulse size in the region
from 2 to 6 Mev. gamma radiation. The maximum gain shift was
reached only after approximately 1/2 hours for a given counting
rate, increasing quickly initially, and approaching an equilibrium
value more slowly. The dependence of this gain shift on pulse
amplitude and dynode H.T. voltage would indicate some dependence
on the instantaneous pulse current drawn not only on the mean
current. This gain shift necessitated frequent calibration
checks when observing the 6 to 10 Mev. region of the spectrum
to ensure that the shift did not mask some of the spectrum struc-
ture. After 20 minutes with a counting rate of 2000 counts per
second above a 0.51 Mev. bias energy with 6.14 Mev. gamma rays
and 1000 volts across the dynode chain the gain increased by
approximately 8 per cent.

(b) Targets.

The target chamber was described in Chapter III. Four
targets of magnetically separated O^{17} layed down on .020 inch
Tungsten backings, were made by A.E.R.E. Harwell England. The
thickness figures supplied with the targets were approximately
50 micrograms per square centimeter for targets number 1 and 2
and 20 and 15 micrograms per square centimeter for targets num-
ber 3 and 4 respectively.

(c) The 872 Kev. Radiation.

Proton bombardment of number 1 and 2 targets at 1.90
Mev. proton energy indicated that there was less than 0.1 micro-

grams per square centimeter of O^{17} assuming the 872 kev. was due to $O^{17}(p,p',\gamma)$. This was calculated from the relative yields of the 872 kev. gamma ray from the separated O^{17} targets and from natural oxygen targets with a known number of oxygen atoms per square centimeter and taking the percentage of O^{17} in natural oxygen as 0.04 per cent. Since an excitation function over the 873 kev. resonance of F^{19} indicated that in these targets there was greater than 0.1 micrograms per square centimeter of Flourine no further search for captive gamma rays from O^{17} was made using these two targets. The number 3 and 4 targets showed no 872 kev. radiation for proton bombarding energies of 1.75 to 2.2 Mev.

An O^{16} target electromagnetically separated by A.E.R.E. Harwell was also bombarded with protons of energy 1.8 to 2.1 Mev. No 872 kev. gamma radiation was observed, however the target contained only a small amount of O^{16} as judged from the yield of γ_2.

(d) Contamination Spectra.

Contamination spectra on target number 3 was studied. An excitation function over the energy range .8 to 1.9 Mev. was measured in 20 kev. intervals. More accurate excitation functions were then made in regions where resonances were indicated. The position of these resonances and the energy of the gamma rays appearing in the spectrum were used to determine the contaminants present. The following nuclear contaminants were found:

F^{19} The yield of 6.14 Mev. gamma rays at the 873 kev. resonance indicated that the amount of F^{19} contamination on the targets was of the order of .1 milli micrograms per square centimeter, much less than that in targets number 1 and 2.

N^{15} Resonances were observed at proton energies of .898 1.2 and 1.650 Mev. with gamma rays of energy 4.41 Mev. This was attributed to $N^{15}(p,\alpha,\gamma)C^{12}$, (Hagedorn and Marion (57) and Schardt et al (52)). The apparent lack of resonances in $N^{14}(p,\gamma)$ of comparable height to the $N^{15}(p,\alpha,\gamma)C^{12}$ resonance indicated that the amount of N^{15} was greater than the natural abundance ratios for nitrogen isotopes would suggest, and therefore possibly was layed down as NH_2^+ at the mass 17 focus of the separator.

C^{13} The $C^{13}(p,\gamma)N^{14}$ reaction has a resonance at 1.76 Mev. proton energy (Ajzenberg and Lauritsen (55)) which was observed as was the 9.18 Mev. gamma ray from the N^{14} decay. The carbon contamination was not introduced onto the target by the beam since clean tungsten backings which had been bombarded for comparable lengths of time showed less C^{13} contamination.

The separated O^{16} target had showed the 1.63 Mev. gamma radiation from $Na^{23}(p,\alpha,\gamma)Ne^{20}$ between 1.9 and 2.0 Mev. proton bombardment energy. There is considerable sodium on this target.

(e) Measurement of annihilation radiation

Since the F^{18} decays by positron emission with a half life of 112 minutes (Blaser (49)), the existence of annihilation radiation following positron decay with a half life of 112 minutes would indicate that F^{18} had been formed. Therefore an attempt was made to detect the decay through a measurement of the counting rate as a function of time after the beam was turned off. The F^{17} produced from $O^{16}(p,\gamma)$ and N^{13} from $C^{12}(p,\gamma)$ would contribute to the annihilation radiation since both also decay by positron emission. However their associated half lives are 66 seconds (Wong ,54) and 10 minutes (Churchill et al ,53) respectively and will not interfere with measurements made of the 2 hour half life of F^{18}.

The annihilation spectrum was observed using coincidence methods, the small crystal detector being used as the second counter. The head amplifier circuit is shown in Figure 5. The output from the small detector was fed to an E.K. Cole 1049A amplifier which in turn fed an Atomic Instruments single channel analyser. The window of the analyser was set to see radiation between the 300 and 600 kev. energy region of the spectrum by using the mercury pulse generator which had been calibrated in

terms of energy with a gamma ray displayed on the kicksorter.
The output of the analyser triggered the gated biased amplifier
through which the pulse from the large crystal passed. The pul-
ses from the large crystal were delayed by approximately 1.5
microseconds going into the Moody amplifier in order to compen-
sate for the delay in the trigger pulse from the single channel
kicksorter.

After a two hour bombardment with approximately 8
microamperes of 1.8 Mev. protons, the target was removed from
the chamber and placed between the two crystals. The annihila-
tion radiation counting rate observed indicated a fast decay
component probably due to F^{17} produced from $O^{16}(p,\gamma)$ reaction
and also a slowly decaying component with a half life of the or-
der of a few hours, possibly due to F^{18} decay. The counting
rate from this long life portion was very small indicating that
the F^{18} yield for the target was very low.

3. Conclusions.

No 872 kev. gamma radiation was observed from proton
bombardment of the separated O^{16} target. Also on two of the four
separated O^{17} targets the 872 kev. gamma ray did appear at the
higher bombarding energies. On the other two (targets numbered
3 and 4) the radiation was not observed; however this is consis-
tent with the very small amount of F^{18} annihilation radiation.
But the amount of O^{16} and O^{17} on the two types of separated tar-
gets appears to be much smaller than Harwell estimated. This was

confirmed for the O^{16} target by comparison of the yield of γ_2

from tungsetn oxide and from the separated target and for O^{17}

by the relatively small amount of 872 kev. for the separated

target compared to a natural oxide target. Therefore, the con-

clusion which could normally be drawn from the presence or ab-

sence of the 872 kev. gamma ray is doubtful in this case because

of the small number of target atoms in the tungsten backings.

The small amounts of oxygen isotopes on the tungsten

targets suggests either that the oxygen is not retained as an

oxide but occluded in the surface and then lost with subsequent

bombardment, or that the percentage of the mass 17 beam in the

electromagnetic separator which is O^{17} is not as large as assumed.

If the first reason is the cause of the difficulty in the sep-

arator, then using barium metal as a backing on which to form

the oxide might be an improvement because barium forms an oxide

more readily than tungsten.

With reference to the second suggestion, Ahnlund et al

(54) mention that for the electromagnetic separation of O^{17} ,

the hydrogen always present in the ion source combines easily

with oxygen to form OH+ OH_2+ OH_3+; this would give large amounts

of $O^{16}H$+ at the mass 17 focus. Ahnlund et al collected the O^{17}

at mass number 31 in the form of $N^{14}O^{17}$, by using gas enriched

in O^{17}(a few per cent) in the ion source mixed with natural ni-

trogen for which the N^{14} to N^{15} ratio is very high. This

resulted in enriched targets in which the composition was approximately 90 per cent $N^{14}O^{17}$, 7 per cent $N^{15}O^{16}$ and less than 3 per cent $C^{13}O^{18}$.

Possibly this is the only method to get reasonable enrichment of O^{17}. Certainly before any useful information about level parameters of F^{18} can be extracted much better targets will have to be obtained.

FIGURE 10 MERCURY PULSE GENERATOR

APPENDIX

Mercury Relay Pulse Generator.

In order to set up the Marconi thirty channel kick-sorter accurately and check the associated gamma ray detecting electronics, a pulse generator whose accuracy and stability was better than 0.1 per cent was required. If the stability of both pulse generator and counter system is good, a gamma ray energy can be determined in terms of settings of the pulse generator voltage which can be related to a gamma ray energy scale using sources with gamma rays of known energies. The shape of the pulse from the pulse generator must approximate that of the pulses due to gamma ray interaction in the detector so that any non-linearity in the electronics due to different pulse shapes will be eliminated. Therefore the possibility of varying the pulse shape of the generator was required. The pulses should be able to be fed into high or low impedance points in order to test at different points of the counting system.

1. Pulse Generator Mark I.

The Mk I model (Figure 10), was designed to produce pulses to be fed into the grid of the head preamplifier cathode follower. This was a high impedance point permitting the design as shown. The integrating time constant was fixed at the rise time of the pulse from a sodium iodide (thallium activated) scintillation counter, 0.25 microseconds, and the fall time was added externally to the generator usually in the input to the head amplifier.

The Western Electric 276 series of relays switch in one direction when the current through the coil becomes greater than +1.5 milliamperes and switch back when the coil current drops to less than -1.5 milliamperes. On the alternate half cycle from the pulse production, the coupling and pulse shaping capacitors were discharged through a 100K resistor; this produced a pulse of opposite polarity approximately one third the amplitude of the desired pulse. Increasing the 100K resistor to reduce the size of this discharge pulse introduced pick up in the moving arm of the relay during the alternate half cycle, adding ripple to the pulse output.

The fifteen turn 100K Helipot Model B had a linearity rating of ± 0.05 per cent. Only 60 cycle repetition rate was available for the mercury switch. The direct current was supplied by a small battery of dry cells.

2. Pulse Generator Mark II.

The Mk II design (Figure 10) was built to provide additional facilities; first, the output pulses can be fed into both low or high impedance points, second, variable rise and fall times, and a larger amplitude range are provided, and third, a motor driven single turn helipot provides voltage rising linearly in time which when chopped by the mercury switch provides a sliding pulse generator for testing the kicksorter. The design was similar to that described by Battel and Chapman (51).

The linearly varying direct current source was pro-
duced by driving a single turn 5K Helipot Model L, (linearity
0.1%), with a synchronous motor and feeding the voltage from the
sliding arm to the pulse shaper. A single turn helipot was
chosen since this eliminates the need for limit and motor rever-
sing switches which are required for a multiturn helipot. The
single turn helipot however does suffer from the fact that an
additional ripple is introduced by the slider passing over the
single turns of wire on the resistor (1800 turns), however for
the present pulse generator this ripple was less than 0.05%
and consequently was negligible. The motor drives the helipot
through a reduction gear at a speed of 6 r.p.m.

The direct current power supply delivered 10 milli-
amperes at 85 volts with 2 millivolts 10 cycle ripple and less
than 1 millivolt 60 cycle ripple, peak to peak, at the input to
the voltage divider. The voltage divider supplied 60, 15, and
6 volt output for the helipot, variable by adjustable "trimpots",
and 50, 30, and 10 volt outputs for the sliding helipot.

The Western Electric 276 series relays used, have the
property that for 1 millisecond after the switching has occurred
all contacts are shorted. This causes a pedestal like pulse to
appear on the tail of the shaped pulse and also when the relay
returns on the alternate half cycles. This could be made small
by increasing the direct current source impedance. But if the
source impedance was too high there would be a relatively large
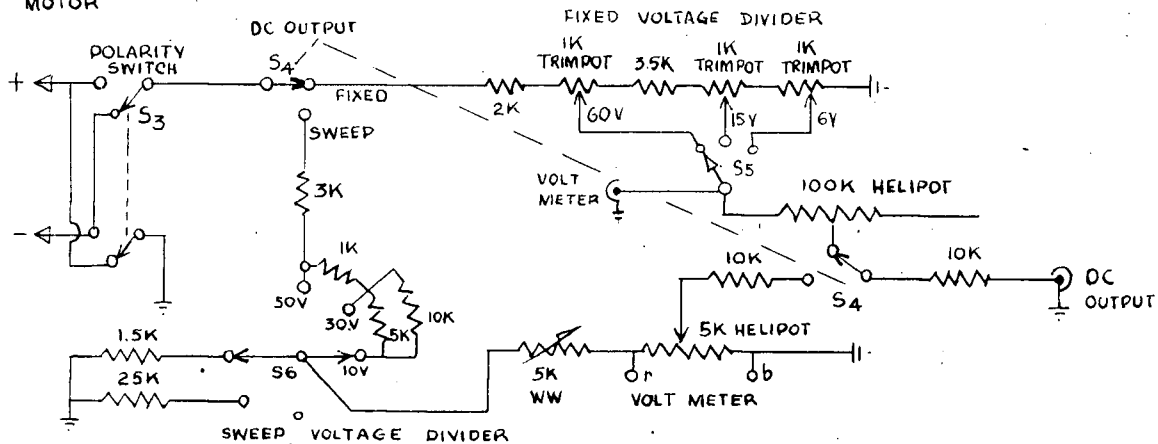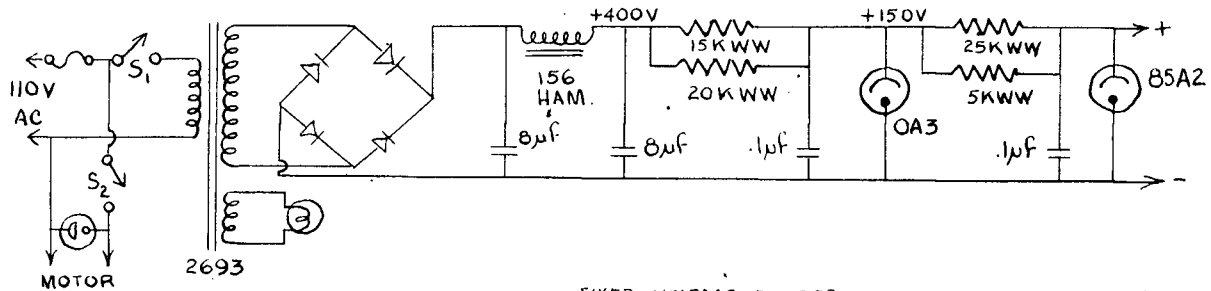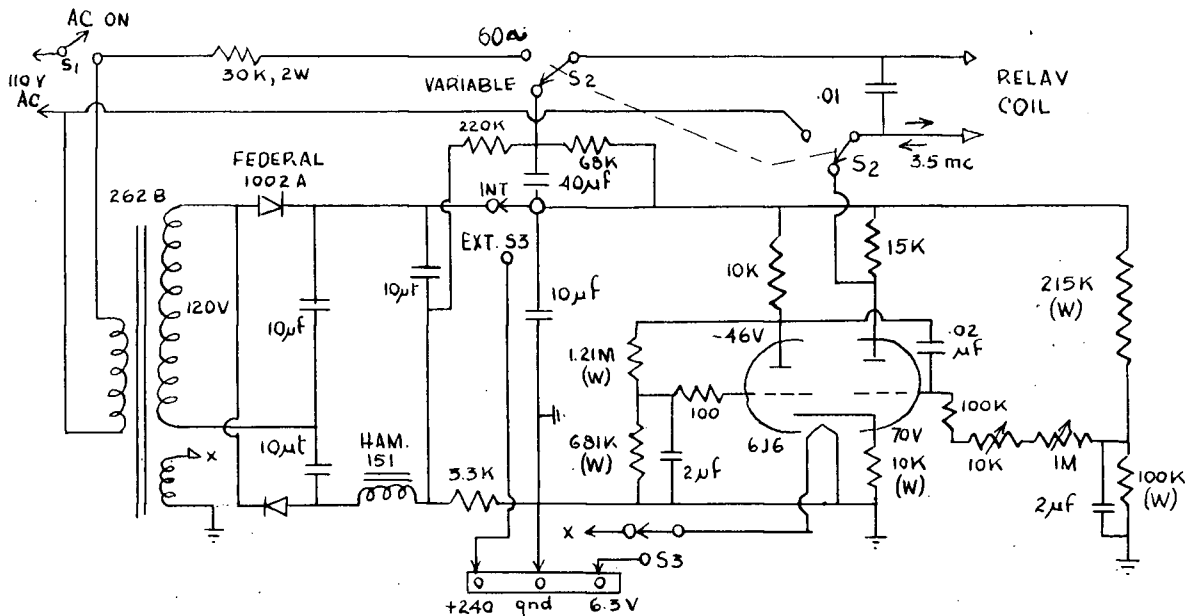
FIGURE II MULTIVIBRATOR CIRCUIT

error in the pulse height produced, due to the charging time of the integrating condenser, which varied with the position of the helipot. This is the reason that a 10K ohm resistor is placed between the direct current output and the helipot, this was the best compromise for minimum pulse due to the relay shorting effect and minimum error due to varying charging time constant. This could be improved by using a 10K ohm helipot and a 100K ohm resistance between the helipot and the direct current output; the time constant error would be negligible and the current pulse would be reduced over that obtained with the circuit shown in Figure 10. The current pulse now causes approximately 1 per cent decrease in d.c. level at 60 volts on the 60 volt range and 0.1 per cent at 6 volts on the 6 volts range. This error is not a linear function of helipot setting for at 56 volts the shift is 0.5 per cent and 0.25 per cent at 40 volts for the 60 volt range.

A multivibrator (Figure 11) was built to permit variable pulse repetion rates to be used. This was introduced not only because of greater flexibility of testing but because in detailed testing of pulse amplitude analysers such as the Marconi 30 channel kicksorter used in this work, if pulses are fed in at mains frequency, then the time correlation between the input pulses and mains frequency ripple voltages in the discriminators may invalidate certain of the results. This effect was confirmed for the present apparatus by noting that if the mercury switch on the sliding pulser (whose linearly rising direct current voltage was produced by the single turn helipot, driven by a synchronous

FIGURE 12   PULSE SHAPE PLOTS OF $e^{-t'}\sinh ct'$
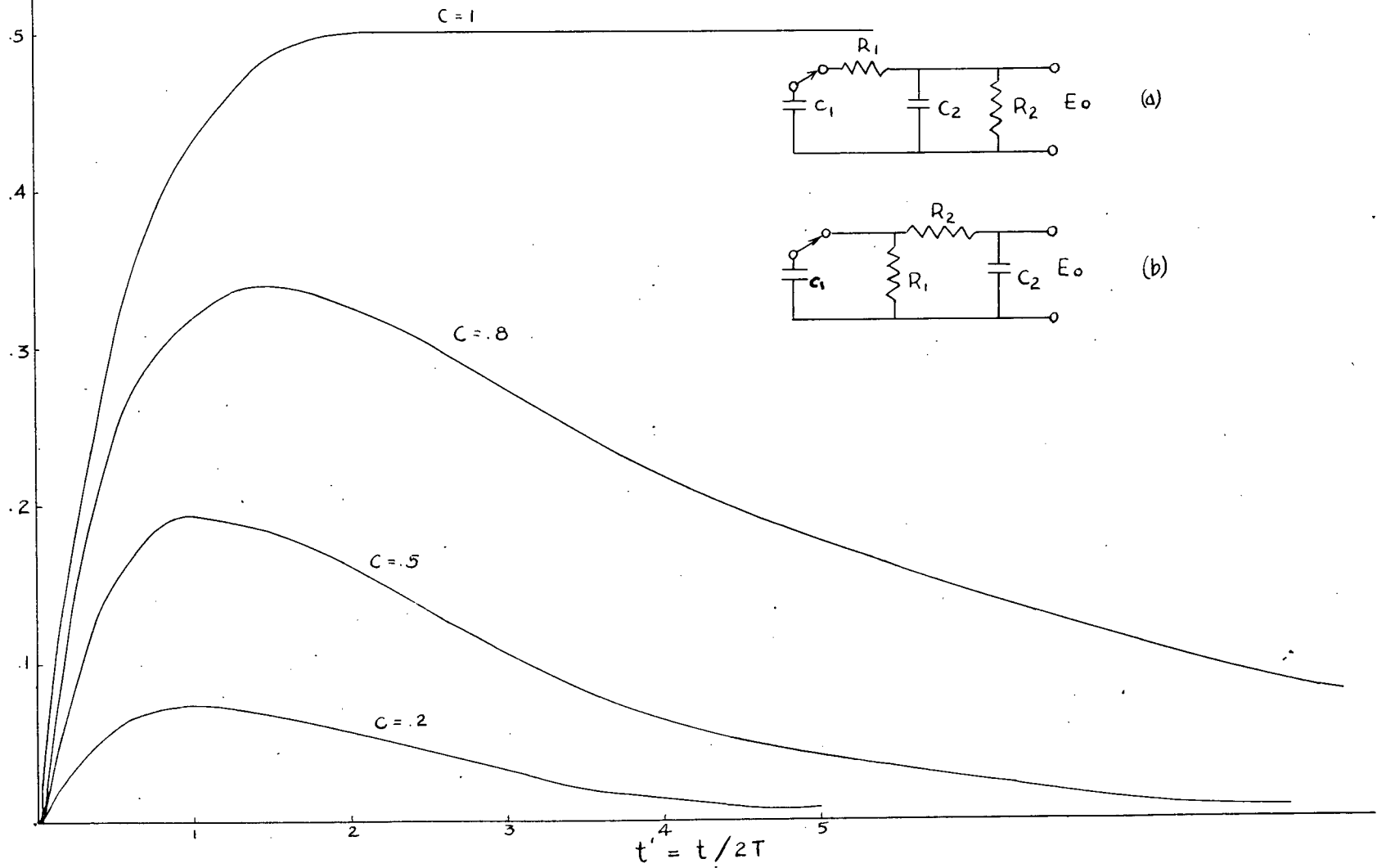
motor and therefore locked to the mains frequency) was run at mains frequency, then the variation in kicksorter channel widths appeared different than when the mercury switch was operated from the multivibrator at a frequency not commensurate with the mains frequency.

The pulse shape is determined by the RC networks used. The response of the circuits can be calculated by using Laplace transform methods. The low impedance, "Lo", output circuit form is essentially that of (a) Figure 12. Solution by Laplace transforms gives

$$e_o(t) = \frac{V_o}{T_2 C} \frac{R_2}{R_1} e^{-t/2T} \sinh \frac{Ct}{2T}$$

where
$$C = \left(1 - \frac{4T^2}{T_1 T_2}\right)^{1/2}$$

$$T_1 = R_1 C_1$$

$$T_2 = R_2 C_2$$

$$\frac{1}{T} = \frac{1}{T_1} + \frac{1}{T_2} + \frac{1}{C_2 R_1}$$

V_o is initial voltage on C_1

Figure 12 shows a plot of exp $-t/2T$ sinh $Ct/2T$. From this plot the rise time is approximately $2T$, nearly independent of C and the fall time constant is approximately $2T/1-C$.

The components were chosen so that feeding into a 75 ohm impedance the "Lo" output would give the time constants indicated on Figure 10.

The "Hi" output circuit is essentially that of (b) Figure 12. If the time constant formed by the coupling condenser and the load is larger than T_1 or T_2 then the voltage at the output $e_o(t)$ is given by:

$$e_o(t) = \frac{V_o}{2T_2C} e^{-t/2T} \sinh Ct/2T$$

which has the same time dependence as above. For the "Hi" output the minimum load impedance which will not affect the time constants is

$$R_L > \frac{R_2C_2}{C_c}$$ where C_c is the size of the output coupling condenser.

The accuracy with which the K.S. can be set up with the sliding popper depends on how the pulse repetition rate and speed of helipot sweep compare.

If the pulses were completely random then about 10,000 counts would have to be accumulated in each channel to set the edges to 1 per cent accuracy (this is what must be done if a compton spectrum from an anthracene crystal is used as a flat spectrum).

If the pulse repetition rate were 60 cycles and the sweep such that 10 counts per sweep per channel were recorded,

then since the sweep helipot is driven by a synchronous motor the channel edges could be set to only 10 per cent no matter how many counts were recorded. Therefore to get 1 per cent accuracy either a sweep speed which permits 100 counts per channel per sweep is necessary or a repetition rate which is a few cycles off 60 cycles.

For this reason the variable frequency drive should be used, set at a frequency close to 60 cycles. This can be checked on an oscilloscope by triggering the sweep at 60 cycles per second and feeding the test pulses into the vertical amplifier. If the test pulse rate is just off 60 cycles per second then the test pulses as seen on the oscilliscope will drift slowly with respect to the horizontal trace.

Bibliography

Ahnlund, K., Thulin, S. and Pauli, R., (1954) Arkiv For Fysik 8, 489.

Ajzenberg, F. and Lauritsen, T., (1955) Rev. Mod. Phys. 27, 77.

Ajzenberg, F., (1951) Phys. Rev. 83, 693.

Alder, F. and Yu, F., (1951) Phys. Rev. 82, 105.

Alexander, T., (1955) M.A. Thesis, University of British Columbia.

Battel, W.J. and Chapman, E,E., (1951) Atomic Energy of Canada Report No CREL-467.

Bethe, H. and Livingstone, M., (1937) Rev. Mod. Phys. 9, 245.

Blaser, Boehm and Marmier (1949 Phys. Rev. 75, 1953.

Bonner, T. and Butler, J., (1951) Phys. Rev. 83, 1091.

Bonner, T. and Marion, J., (1955) Phys. Rev. 100, 46.

Burling, R., (1941) Phys. Rev. 60, 340.

Burrows, Gibson and Rotblat, (1950) Phys. Rev. 80, 1095.

Cameron, A. (1957) Atomic Energy of Canada, A.E.C.L. No 454, Report No CRL-41.

Churchill, Jones, and Hunt, (1953) Nature 172, 460.

Dosso, H., (1957) M.A. Thesis, University of British Columbia.

Doyle, W. and Robbins, A., (1956) Phys. Rev. 101, 1056.

DuBridge, S., Barnes, S., Buck, J. and Strain, C., (1938) Phys. Rev. 53, 447.

Edwards, M., (1950) M.A. Thesis, University of British Columbia.

Hagedorn, F. and Marion, J. - Kellog Radiation Lab. Preprint.

Hirschfelder, J. and Magee, J., (1948) Phys. Rev. 73, 207.

Larson, E., (1957) M.A. Thesis, University of British Columbia

Laubenstein, R. and Laubenstein, M., (1951) Phys. Rev. 84, 18.

Laubenstein, R., Laubenstein, M., Koester, L. and Mobley, R.,
    (1951) Phys. Rev. $\underline{84}$, 12.

Salpeter, E., (1955) Astrophysical J. $\underline{121}$, 161.

Schardt, Fowler and Lauritsen, (1952) Phys. Rev. $\underline{86}$, 527.

Stelson, P. and McGowan, F., (1955) Phys. Rev. $\underline{99}$, 112.

Stelson, P. and Preston, (1954) Phys. Rev. $\underline{95}$, 974.

Thirion, J., (1953) Annales de Physique $\underline{8}$, 489.

Thomas, R. and Lauritsen, T., (1952) Phys. Rev. $\underline{88}$, 469.

Van Allen, J. and Smith, N., (1941) Phys. Rev. $\underline{59}$, 618

Warren, J., Laurie, K., James, D. and Erdman, K., (1954) Can. J.
    Phys. $\underline{32}$, 563.

Wenzel, W. and Whaling, W., (1952) Phys. Rev. $\underline{87}$, 499.

Whaling, W., (1957) Kellog Radiation Laboratory Preprint.

Wong, C., (1954) Phys. Rev. $\underline{95}$, 761.